

EXCITATION AND PROPAGATION OF WAVES
BETWEEN TWO PLANAR INTERFACES

by
Yu-Ping Liu

A dissertation submitted in partial fulfillment
of the requirements for the degree of
Doctor of Philosophy
(Electrical Engineering)
in The University of Michigan
1973

Doctoral Committee:

Professor Chen-To Tai, Co-Chairman
Professor Chiao-Min Chu, Co-Chairman
Professor Vi-Cheng Liu
Professor Charles B. Sharpe
Dr. Dipak L. Sengupta

ABSTRACT

EXCITATION AND PROPAGATION OF WAVES BETWEEN TWO PLANAR INTERFACES

by
Yu-Ping Liu

Co-Chairmen: Chen-To Tai, Chiao-Min Chu

The theoretical study of wave propagation in the free space region between two parallel planar interfaces is presented. The upper part of the region is bounded by a perfectly conducting plate while the lower part is bounded by a lossy dielectric earth. The dyadic Green's function for this geometry is developed as an Ohm-Rayleigh type of expansion in terms of the Hansen vector wave functions. This dyadic Green's function is used to obtain the field expressions for Hertzian dipoles of electric and magnetic type with different orientations. Methods of evaluating the integral expression for the fields are studied in great detail.

The pole contributions from the integral representation of the field yield the modal picture of the surface wave. The excitation factor and the mode function for the wave expressions are derived. The dependence of the real and imaginary parts of the poles on the property of the lossy dielectric medium is discussed.

By means of the deformation of integration contour and the saddle point method, the far field expressions for the waves excited by different elementary sources are derived. The proper choice of branch cut in performing the contour integral is discussed.

Some numerical results are presented in graphical form. The results obtained by using the Leontovich impedance boundary condition on the lossy interface are compared with the exact results obtained by using the continuity of tangential fields across the interface. The symmetry properties of the dyadic Green's function in a two layer problem are investigated.

ACKNOWLEDGMENTS

I wish to express my appreciation to all the members of my doctoral committee for their comments. My deep indebtedness is given to Professor Chen-To Tai who suggested the area of research and provided continuous inspiration, guidance and encouragement. Also special thanks are due Professor Chiao-Min Chu for his advice and valuable criticism.

Thanks are also due Dr. Harold E. Foster, Dr. Adel Mohsen and Mr. Gerard Desjardins for their helpful discussion. The careful typing of Mrs. Karen L. Christiansen is appreciated.

Finally, I would like to take this chance to express my appreciation to my wife, Chi-ling, for her understanding and patient consideration during the course of study.

TABLE OF CONTENTS

	ii
ACKNOWLEDGMENTS	ii
LIST OF TABLES	v
LIST OF ILLUSTRATIONS	vi
LIST OF APPENDICES	vii
I INTRODUCTION	1
II DYADIC GREEN'S FUNCTIONS	4
2.1 General Remarks	4
2.2 Free Space Green's Function	4
2.3 Composition of Green's Function for Electric Dipoles	6
2.4 Composition of Green's Function for Magnetic Dipoles	9
2.5 Symmetry Property of Dyadic Green's Function	12
2.6 Impedance Boundary Condition	17
2.7 Approximate Dyadic Green's Function Satisfying the Impedance Boundary Condition	17
2.8 Relationship Between Exact and Approximate Green's Function	20
III FIELDS DUE TO HERTZIAN DIPOLES	21
3.1 <u>Introduction</u>	21
3.2 z-directed Dipole	21
3.2.1 Integral Representation	21
3.2.2 Asymptotic Solution	23
3.2.3 Comparison with Mode Theory Results	27
3.2.4 Leontovich Approximate Solution	29
3.3 x-directed Dipole	30
3.3.1 Exact Solution	30
3.3.2 Leontovich Approximate Solution	32
3.4 Horizontal Current Loop	32
3.5 Vertical Current Loop	33
IV CALCULATION AND DISCUSSION OF RESULTS	34
4.1 <u>General Remarks</u>	34
4.2 Percentage Error by Using Impedance Boundary Condition	34
4.3 Far-Zone Field	40
4.4 Distribution of Poles in Complex θ Domain	46
4.5 Excitation Factor for Various Sources	49

V	CONCLUSIONS AND RECOMMENDATIONS	54
5.1	Conclusions	54
5.2	Areas for Future Study	54
	REFERENCES	56
	APPENDICES	58

LIST OF TABLES

Table		Page
4-1	Refractive Index for Different Frequency	35
4-2	Percentage Error of Reflection Coefficients	36
4-3	Percentage Error for Far Field	46
4-4	Table of Excitation Factor for Wave Components for Different Sources	48
4-5	Location of Poles for Good Earth	50
4-6	Location of Poles for Poor Earth	50

LIST OF APPENDICES

APPENDIX A: General Discussion on Saddle Point Integration	58
APPENDIX B: Newton-Raphson's Method	64
APPENDIX C: Discussion of Pole Distribution	66
APPENDIX D: Computer Program	<hr/> 70

LIST OF ILLUSTRATIONS

Figure		Page
1-1	Geometric Configuration	1
3-1	Path of Integration in Complex λ Plane	25
3-2	Path of Integration in Complex β Plane	25
4-1	Magnitude of Reflection Coefficient at 6 MHz	37
4-2	Magnitude of Reflection Coefficient at 600 KHz	38
4-3	Magnitude of Reflection Coefficient at 60 KHz	39
4-4	Far-Zone Electric Field of Unit Dipole Moment at 6 MHz	41
4-5	Far-Zone Electric Field of Unit Dipole Moment at 600 KHz	42
4-6	Far-Zone Electric Field of Unit Dipole Moment at 60 KHz	43
4-7	Far-Zone Electric Field of Unit Dipole Moment at 6 MHz ($z_0 = 5 \text{ m}$)	44
4-8	Far-Zone Electric Field of Unit Dipole Moment at 6 MHz ($z_0 = 25 \text{ m}$)	45
4-9	Pole Distribution for Good Earth	51
4-10	Pole Distribution for Poor Earth	52
A-1	Branch Cut Along $\text{Re } \sqrt{k^2 - \lambda^2} = 0$	58
A-2	Branch Cut Along $\text{Im } \sqrt{k^2 - \lambda^2} = 0$	59
A-3	Branch Cut Parallel to Imaginary Axis	60
A-4	Integration Path in Complex β Plane	61
C-1	Pole Locus at Cut-Off Frequency	67
C-2	Pole Locus Above Cut-Off Frequency	69

ABSTRACT

EXCITATION AND PROPAGATION OF WAVES BETWEEN TWO PLANAR INTERFACES

by
Yu-Ping Liu

Co-Chairmen: Chen-To Tai, Chiao-Min Chu

The theoretical study of wave propagation in the free space region between two parallel planar interfaces is presented. The upper part of the region is bounded by a perfectly conducting plate while the lower part is bounded by a lossy dielectric earth. The dyadic Green's function for this geometry is developed as an Ohm-Rayleigh type of expansion in terms of the Hansen vector wave functions. This dyadic Green's function is used to obtain the field expressions for Hertzian dipoles of electric and magnetic type with different orientations. Methods of evaluating the integral expression for the fields are studied in great detail.

The pole contributions from the integral representation of the field yield the modal picture of the surface wave. The excitation factor and the mode function for the wave expressions are derived. The dependence of the real and imaginary parts of the poles on the property of the lossy dielectric medium is discussed.

By means of the deformation of integration contour and the saddle point method, the far field expressions for the waves excited by different elementary sources are derived. The proper choice of branch cut in performing the contour integral is discussed.

Some numerical results are presented in graphical form. The results obtained by using the Leontovich impedance boundary condition on the lossy interface are compared with the exact results obtained by using the continuity of tangential fields across the interface. The symmetry properties of the dyadic Green's function in a two layer problem are investigated.

CHAPTER I

INTRODUCTION

The purpose of this thesis is to theoretically study electromagnetic wave propagation in the vicinity of two parallel plates of different material. In particular, one plate considered is the lossy ground plane; the other is the perfectly conducting screen above it.

Two major steps are involved in the calculation of the far-zone field of a transmitting antenna. First, the integral expressions for the electromagnetic fields need to be derived by using the dyadic Green's function technique. Secondly, the integration involved is carried out by the saddle point integration method.

The geometry of the problem considered is illustrated in Fig. 1-1. The

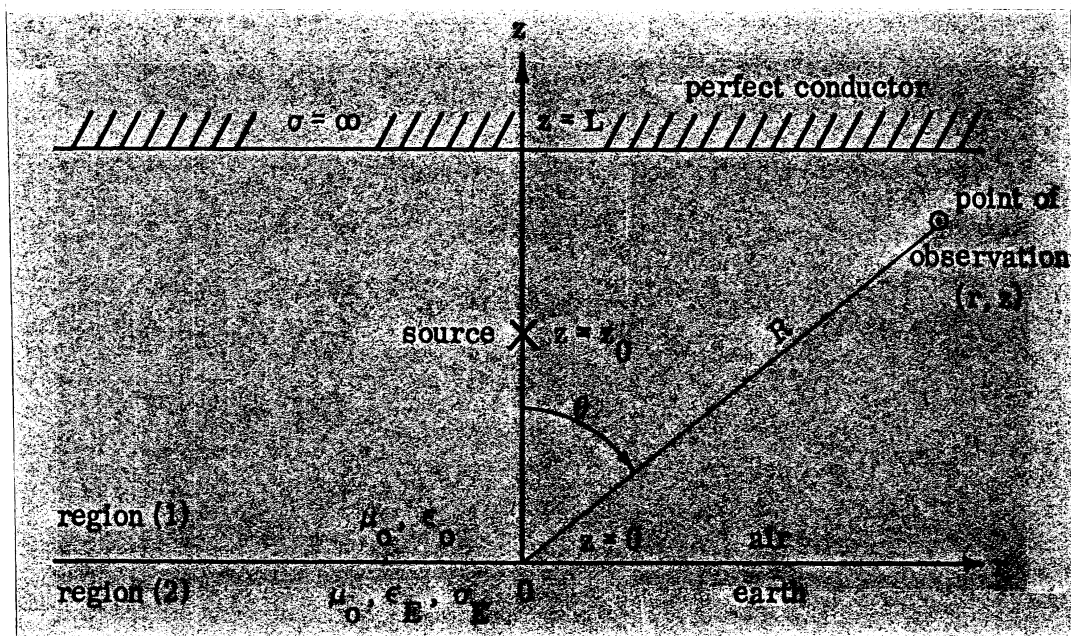


FIG. 1-1: GEOMETRIC CONFIGURATION

dipole is located at a height z_0 above the earth. The earth is considered to be a homogeneous medium with finite conductivity as in Sommerfeld's problem [16]. The distance between the perfectly conducting top plate and the earth is L which

is larger than z_0 . The medium in between the plates is free space.

The problem of finding the electromagnetic wave propagation between the ionosphere and the earth has been discussed by many authors. Watson [1] considered it as a propagating waveguide of electromagnetic wave. He employed a waveguide approach (between an idealized homogeneous earth and a concentric reflecting layer) in which he devised the celebrated transformation in rapid convergence. The same model with certain refinements has been discussed by many others; in particular, Bremmer [2], Budden [3, 4], Wait [5] compiled many useful results in book form, utilizing either mode theory or Hertzian potential technique. In general, they considered the earth as highly conductive.

The problem discussed here, unlike the ionosphere problem of low frequency and large distance, involves high frequencies and a very short separation distance. However, both have similar configurations.

In this dissertation the method used to calculate the fields is that of the dyadic Green's function. The derivation follows the scattering superposition scheme suggested by Tai [6, 7]. The use of the dyadic Green's function technique to solve the wave propagation problem provides a general treatment of both excitation and wave mode at the same time. The exact integral representation of the field is obtained by using composite dyadic Green's functions. The integration is treated by the saddle point method. Thus, the solution at a large distance from the source is investigated. In contrast, the mode theory approach requires consideration of the excitation factor separately or a special source function must be chosen to obtain the right kind of potential.

In Chapter II the dyadic Green's functions for mixed boundary conditions are found. Two kinds of Green's functions are needed for two different sources. When the material is highly conductive, an approximate impedance boundary condition is imposed on the lossy earth. The usage of the Leontovich boundary condition replacing the exact tangential continuous condition is termed as the approximate solution. A symmetry property is derived for the two layer prob-

lem in our research.

In Chapter III the fields due to Hertzian dipoles are derived. The dipole sources considered are of electric and magnetic type with both horizontal and vertical orientation. The far-field is evaluated by means of the saddle point method. The results obtained by the method of Green's functions are compared with the mode theory of the waveguide.

Chapter IV contains the results of various computer aided numerical calculations. The ground parameters were chosen to be representative of those actually encountered in practice. Several frequencies were chosen to study the nature of the ground. Some overlooked comments on wave propagation in the literature are discussed. The error in the results when using the impedance boundary condition is found. The advantages of using the dyadic Green's function technique are shown by eliminating the determination work on the choice of Hertzian potentials and the excitation factors. A general discussion of mode distribution is included.

In Chapter V the conclusions as well as suggested areas where future efforts may be productive are discussed.

CHAPTER II

DYADIC GREEN'S FUNCTIONS

2.1 General Remarks

The dyadic Green's function technique for treating electromagnetic boundary-value problems was first formulated by Schwinger [8] in 1943. Levine and Schwinger [9] used this method to solve the problem of diffraction by an aperture. In their book, Morse and Feshbach [10] introduced the free-space dyadic Green's functions by way of the vector Helmholtz equation. In 1954, Tai [11] collected his work on these functions into a report which was developed further and published in book form in 1972 [6].

The general procedure for finding the Green's function related to a particular problem is discussed in great detail in Tai's book. In this thesis, we apply the method of Ohm-Rayleigh to a configuration as shown in Fig. 1-1. We consider only harmonically varying fields. The time factor $e^{-i\omega t}$ is applied in this work.

2.2 Free Space Green's Functions

In dealing with the integral representation of fields in free space, the cylindrical vector wave function used has continuous eigenvalues in the λ -domain as well as in the h -domain, where λ is related to the radial eigenfunction and h is related to the longitudinal eigenfunction. The free space Green's function for the same type of problems is developed by Tai [6]. The method used is the Ohm-Rayleigh or eigenfunction expansion technique. In cylindrical coordinates, the free-space dyadic Green's function is given by [6], [7]:

$$\bar{G}_0(\bar{R}/\bar{R}') = \frac{i}{4\pi} \int_0^\infty \frac{d\lambda}{\lambda} \sum_{n=0}^{\infty} \frac{2 - \delta_0}{h} \left\{ \begin{array}{l} \bar{M}_{e_{0n\lambda}}^{(h)} \bar{M}'_{e_{0n\lambda}}^{(-h)} + \\ \bar{M}_{e_{0n\lambda}}^{(-h)} \bar{M}'_{e_{0n\lambda}}^{(h)} + \\ \bar{N}_{e_{0n\lambda}}^{(h)} \bar{N}'_{e_{0n\lambda}}^{(-h)} \\ + \bar{N}_{e_{0n\lambda}}^{(-h)} \bar{N}'_{e_{0n\lambda}}^{(h)} \end{array} \right\} - \bar{I}_t \frac{\delta(\bar{R} - \bar{R}')}{k^2} \quad (2.1)$$

$z > z'$
 $z < z'$

where

$$\bar{I}_t = \hat{z} \hat{z}$$

k : the free space wave number $= \sqrt{\lambda^2 + h^2}$

λ : eigenvalue pertaining to the radial function

h : eigenvalue pertaining to the longitudinal function

$$\delta_0 = \begin{cases} 1 & n = 0 \\ 0 & n \neq 0 \end{cases} \quad \text{Kronecker delta function}$$

and the vector wave functions are defined as:

$$\begin{aligned} \bar{M}_{e n \lambda}^{(\pm h)} &= \nabla_x \left[J_n(\lambda r) \begin{cases} \cos n\phi e^{\pm i h z} \hat{z} \\ \sin n\phi e^{\pm i h z} \hat{z} \end{cases} \right] \\ &= \left[\mp \frac{n J_n(\lambda r)}{r} \begin{cases} \sin n\phi \hat{r} \\ \cos n\phi \hat{r} \end{cases} - \frac{\partial J_n(\lambda r)}{\partial r} \begin{cases} \cos n\phi \hat{\theta} \\ \sin n\phi \hat{\theta} \end{cases} \right] e^{\pm i h z} \\ \bar{N}_{e n \lambda}^{(\pm h)} &= \frac{1}{k} \nabla_x \bar{M}_{e n \lambda}^{(\pm h)} \\ &= \frac{1}{k} \left[i(\pm h) \frac{\partial J_n(\lambda r)}{\partial r} \begin{cases} \cos n\phi \hat{r} \\ \sin n\phi \hat{r} \end{cases} \mp \frac{i(\pm h)n}{r} J_n(\lambda r) \begin{cases} \sin n\phi \hat{\theta} + \lambda^2 J_n(\lambda n) \cos n\phi \hat{z} \\ \cos n\phi \hat{\theta} \end{cases} \right] e^{\pm i h z} \quad (2.2) \end{aligned}$$

The subscript e corresponds to even angular functions, and $(\pm h)$ corresponds to odd $e^{-\pm i h z}$ and $J_n(\lambda r)$ is the n th order Bessel function.

A simplified notation for the sum has been adopted:

$$\bar{M}_{e n \lambda}^{(h)} \bar{M}'_{e n \lambda}^{(-h)} = \bar{M}_{e n \lambda}^{(h)} \bar{M}'_{e n \lambda}^{(-h)} + \bar{M}_{o n \lambda}^{(h)} \bar{M}'_{o n \lambda}^{(-h)}$$

$$\bar{N}_{e n \lambda}^{(h)} \bar{N}'_{e n \lambda}^{(-h)} = \bar{N}_{e n \lambda}^{(h)} \bar{N}'_{e n \lambda}^{(-h)} + \bar{N}_{o n \lambda}^{(h)} \bar{N}'_{o n \lambda}^{(-h)} .$$

The \bar{M}' and \bar{N}' functions are defined in the primed coordinate system, the source coordinates \bar{R}' . For these vector wave functions, the sign of $h = \pm \sqrt{k^2 - \lambda^2}$ is chosen so that the imaginary part is always positive throughout the calculations; this insures that the radiation condition is always satisfied.

The free space Green's function is the basic building block in the method

of scattering superposition [6], [7].

2.3 Composition of Green's Function for Electric Dipoles

The plane earth is assumed to be a homogeneous lossy dielectric with a permeability μ_0 equal to that of free space, a relative permittivity ϵ_E , and a finite conductivity σ_E . Associated with the lossy earth is the following propagation constant.

$$k_E^2 = k_0^2 \left(\frac{\epsilon_E}{\epsilon_0} + i \frac{\sigma_E}{\omega \epsilon_0} \right) \quad \text{where } k_0^2 = \omega^2 \mu_0 \epsilon_0 .$$

The complex index of refraction is defined as

$$n^2 = \frac{\epsilon_E}{\epsilon_0} + i \frac{\sigma_E}{\omega \epsilon_0} .$$

The new Green's function can be found in the following way. For convenience, the coordinates are picked so the perfect conductor is at $z = 0$ while the lossy earth is located at $z = L$. Applying the technique of scattering superposition, the dyadic Green's function of the first kind with perfect conductor at $z = 0$ is:

$$\bar{\bar{G}}_1(\bar{R}/\bar{R}') = \bar{\bar{G}}_0(\bar{R}/\bar{R}') + \bar{\bar{G}}_{1S}(\bar{R}/\bar{R}') \quad z > 0 \quad (2.3)$$

where $\bar{\bar{G}}_0$ is as previously defined and

$$\bar{\bar{G}}_{1S} = \frac{i}{4\pi} \int_0^\infty \frac{d\lambda}{\lambda} \sum_{n=0}^\infty \frac{2 - \delta_0}{h} \left[a \bar{M}_{e_n \lambda}^{(h)} \bar{M}'_{e_n \lambda}^{(h)} + b \bar{N}_{e_n \lambda}^{(h)} \bar{N}'_{e_n \lambda}^{(h)} \right] .$$

Here a and b are two unknown constants which are specified by the boundary conditions. The posterior elements are guided by the expression of $\bar{\bar{G}}_0$ which has to be the same as the part of $\bar{\bar{G}}_0$ when $z < z'$ and the anterior elements are dictated by the nature of the reflected outgoing wave. Notice that the singular term at source point has been dropped since the singular nature of $\bar{\bar{G}}_1$ is taken care of by $\bar{\bar{G}}_0$.

The boundary condition at $z = 0$ requires that:

$$\hat{z} \times \bar{\bar{G}}_1 = 0 \quad . \quad (2.4)$$

Substituting Eqs. (2.1), (2.2) and (2.3) into (2.4) yields:

$$a = -1 \quad b = 1 \quad .$$

Thus the complete expression for the dyadic Green's function of the first kind is:

$$\begin{aligned} \bar{\bar{G}}_1(\bar{R}/\bar{R}') &= \frac{i}{4\pi} \int_0^\infty \frac{d\lambda}{\lambda} \sum_{n=0}^{\infty} \frac{2-\delta_o}{h} \left\{ \begin{array}{l} \bar{M}(h) \bar{M}'(-h) - \bar{M}(h) \bar{M}'(h) + \bar{N}(h) \bar{N}'(-h) + \\ \bar{M}(-h) \bar{M}'(h) - \bar{M}(h) \bar{M}'(h) + \bar{N}(-h) \bar{N}'(h) + \\ + \bar{N}(h) \bar{N}'(h) \end{array} \right\} \quad z > z' \\ &\quad + \bar{N}(h) \bar{N}'(h) \quad 0 \leq z < z' \end{aligned}$$

where the abbreviated form of $\bar{M}_{e_{o n \lambda}}(h)$ and $\bar{N}_{e_{o n \lambda}}(h)$ represented by $\bar{M}(h)$ and $\bar{N}(h)$ have been used to simplify the notation.

Now the dyadic Green's function of the third kind needed for the problem can be constructed from that of the first kind, using the method of scattering superposition. In order to satisfy the radiation condition and the boundary conditions at the interfaces, the Green's function is assumed to have the following form

$$\begin{aligned} \bar{\bar{G}}_3^{(11)}(\bar{R}/\bar{R}') &= \frac{i}{4\pi} \int_0^\infty \frac{d\lambda}{\lambda} \sum_{n=0}^{\infty} \frac{2-\delta_o}{h} \left\{ \begin{array}{l} \bar{M}(h) \left[\bar{M}'(-h) - \bar{M}'(h) \right] + \bar{N}(h) \left[\bar{N}'(-h) + \bar{N}'(h) \right] + \\ \left[\bar{M}(-h) - \bar{M}(h) \right] \bar{M}'(h) + \left[\bar{N}(-h) + \bar{N}(h) \right] \bar{N}'(h) + \\ + \bar{R}_e \left[\bar{M}(-h) - \bar{M}(h) \right] \left[\bar{M}'(-h) - \bar{M}'(h) \right] + \bar{R}_m \left[\bar{N}(-h) + \bar{N}(h) \right] \left[\bar{N}'(-h) + \bar{N}'(h) \right] \end{array} \right\} \quad L \geq z > z' \\ &\quad + \bar{R}_e \left[\bar{M}(-h) - \bar{M}(h) \right] \left[\bar{M}'(-h) - \bar{M}'(h) \right] + \bar{R}_m \left[\bar{N}(-h) + \bar{N}(h) \right] \left[\bar{N}'(-h) + \bar{N}'(h) \right] \quad z' > z \geq 0 \end{aligned} \quad (2.5)$$

$$\begin{aligned} \bar{\bar{G}}_3^{(21)}(\bar{R}/\bar{R}') &= \frac{i}{4\pi} \int_0^\infty \frac{d\lambda}{\lambda} \sum_{n=0}^{\infty} \frac{2-\delta_o}{h} \left\{ \begin{array}{l} T_e \bar{M}(h_E) \left[\bar{M}'(-h) - \bar{M}'(h) \right] + \\ + T_m \bar{N}(h_E) \left[\bar{N}'(-h) + \bar{N}'(h) \right] \end{array} \right\} \quad z \geq L \end{aligned}$$

where

$$h_E = \pm \sqrt{k_E^2 - \lambda^2} .$$

The first superscript (2) implies that \bar{R} is in medium 2 and the second superscript 1 means that \bar{R}' is in medium 1. R_e , R_m , T_e and T_m are four unknown coefficients to be determined. The boundary conditions at the dielectric surface which are used to determine the unknown coefficients are:

$$\hat{z} \times \bar{G}_3^{(11)}(\bar{R}/\bar{R}') = \hat{z} \times \bar{G}_3^{(21)}(\bar{R}/\bar{R}') \Big|_{z=L}$$

$$\hat{z} \times \nabla \times \bar{G}_3^{(11)}(\bar{R}/\bar{R}') = \hat{z} \times \nabla \times \bar{G}_3^{(21)}(\bar{R}/\bar{R}') \Big|_{z=L} .$$

We have assumed $\mu_0 = \mu_1 = \mu_2$. Substituting (2.5) into the above equations we obtain:

$$e^{ihL} + R_e \left[e^{-ihL} - e^{ihL} \right] = T_e e^{ih_E L}$$

$$\frac{h}{k} e^{ihL} + R_m \left[-\frac{h}{k} e^{-ihL} + \frac{h}{k} e^{ihL} \right] = T_m \frac{h_E}{k_E} e^{ih_E L}$$

$$h e^{ihL} + R_e \left[-h e^{-ihL} - h e^{ihL} \right] = T_e h_E e^{ih_E L}$$

$$k e^{ihL} + R_m \left[k e^{-ihL} + k e^{ihL} \right] = T_m k_E e^{ih_E L} .$$

These linear equations yield

$$R_e = \frac{(h - h_E) e^{ihL}}{2 [h \cos(hL) - i h_E \sin(hL)]} \quad (2.6)$$

$$T_e = \frac{h e^{-ih_L}}{h \cos(hL) - i h_E \sin(hL)} \quad (2.7)$$

$$R_m = \frac{(hk_E^2 - h_E k^2) e^{ihL}}{2 \left[k^2 h_E^2 \cos(hL) - ik_E^2 h \sin(hL) \right]} \quad (2.8)$$

$$T_m = \frac{h k k_E e^{-ih_E L}}{k^2 h_E^2 \cos(hL) - ik_E^2 h \sin(hL)} \quad . \quad (2.9)$$

Knowing the complete expression of $\bar{\bar{G}}_3$, we can calculate the electric field due to a known current source by

$$\bar{E}(\bar{R}) = i\omega\mu_0 \iiint \bar{\bar{G}}_3^{(11)}(\bar{R}/\bar{R}') \cdot \bar{J}(\bar{R}') dV' \quad L \geq z \geq 0 ,$$

$$\bar{E}(\bar{R}) = i\omega\mu_0 \iiint \bar{\bar{G}}_3^{(21)}(\bar{R}/\bar{R}') \cdot \bar{J}(\bar{R}') dV' \quad z \geq L ,$$

2.4 Composition of Green's Function for Magnetic Dipoles

In principle, once the appropriate dyadic Green's function is known, the electromagnetic field due to any arbitrary current distribution can be found by evaluating the definite integrals involving the current distribution. In practice, for currents in the form of small loops it is more convenient to use the alternative choice of boundary condition. By introducing an equivalent magnetization vector \bar{m} in place of the current \bar{J} , the vector wave equation for H becomes

$$\nabla \times \nabla \times \bar{H} - k^2 \bar{H} = k^2 \bar{m} \quad . \quad (2.10)$$

The magnetization vector \bar{m} is defined as

$$\bar{m} = I \bar{A} ,$$

where I denotes an equivalent loop current and \bar{A} the vectorial area of the loop.

To solve Eq. (2.10) directly, it is convenient to construct a G_2 function which satisfies the boundary condition $\hat{n} \times \nabla \times \bar{\bar{G}}_2 = 0$. The procedure is exactly the same as before. The dyadic Green's function of the second kind

with a perfect conductor at $z = 0$ is

$$\bar{\bar{G}}_2(\bar{R}/\bar{R}') = \bar{\bar{G}}_0(\bar{R}/\bar{R}') + \bar{\bar{G}}_{2S}(\bar{R}/\bar{R}') \quad z \geq 0 \quad (2.11)$$

where

$$\bar{\bar{G}}_{2S} = \frac{i}{4\pi} \int_0^\infty \frac{d\lambda}{\lambda} \sum_{n=0}^{\infty} \frac{2-\delta_o}{h} \left[c \bar{M}(h) \bar{M}'(h) + d \bar{N}(h) \bar{N}'(h) \right].$$

The boundary condition at $z = 0$ requires that

$$\hat{z} \times \nabla_x \bar{\bar{G}}_2 = 0. \quad (2.12)$$

Substituting Eqs. (2.1), (2.2) and (2.11) into (2.12) yields the constants c and d :

$$c = 1, \quad d = -1.$$

Thus, the $\bar{\bar{G}}_2$ function is given by

$$\bar{\bar{G}}_2(\bar{R}/\bar{R}') = \frac{i}{4\pi} \int_0^\infty \frac{d\lambda}{\lambda} \sum_{n=0}^{\infty} \frac{2-\delta_o}{h} \left\{ \begin{array}{l} \bar{M}(h) \bar{M}'(-h) + \bar{M}(h) \bar{M}'(h) + \bar{N}(h) \bar{N}'(-h) - \bar{N}(h) \bar{N}'(h) \\ \bar{M}(-h) \bar{M}'(h) + \bar{M}(h) \bar{M}'(h) + \bar{N}(-h) \bar{N}'(h) - \bar{N}(h) \bar{N}'(h) \end{array} \right. \begin{array}{l} z > z' \\ z' > z > 0 \end{array} .$$

Now, with the dielectric earth on top at $z = L$, the Green's function of the fourth kind must have the form

$$\begin{aligned} \bar{\bar{G}}_4^{(11)}(\bar{R}/\bar{R}') = & \frac{i}{4\pi} \int_0^\infty \frac{d\lambda}{\lambda} \sum_{n=0}^{\infty} \frac{2-\delta_o}{h} \left\{ \begin{array}{l} \bar{M}(h) \left[\bar{M}'(-h) + \bar{M}'(h) \right] + \bar{N}(h) \left[\bar{N}'(-h) - \bar{N}'(h) \right] \\ \left[\bar{M}(-h) + \bar{M}(h) \right] \bar{M}'(h) + \left[\bar{N}(-h) - \bar{N}(h) \right] \bar{N}'(h) \end{array} \right. \\ & + S_m \left[\bar{M}(-h) + \bar{M}(h) \right] \left[\bar{M}'(-h) + \bar{M}'(h) \right] + S_e \left[\bar{N}(-h) - \bar{N}(h) \right] \left[\bar{N}'(-h) - \bar{N}'(h) \right] \left. \right\} L \geq z > z' \\ & + S_m \left[\bar{M}(-h) + \bar{M}(h) \right] \left[\bar{M}'(-h) + \bar{M}'(h) \right] + S_e \left[\bar{N}(-h) - \bar{N}(h) \right] \left[\bar{N}'(-h) - \bar{N}'(h) \right] \left. \right\} z' > z \geq 0 \end{aligned} \quad (2.13)$$

$$\bar{\bar{G}}_4^{(21)}(\bar{R}/\bar{R}') = \frac{i}{4\pi} \int_0^\infty \frac{d\lambda}{\lambda} \sum_{n=0}^{\infty} \frac{2-\delta_o}{h} \left\{ P_m \bar{M}(h_E) \left[\bar{M}'(-h) + \bar{M}'(h) \right] + P_e \bar{N}(h_E) \left[\bar{N}'(-h) - \bar{N}'(h) \right] \right\} \quad z \geq L$$

where

$$h_E = \pm \sqrt{k_E^2 - \lambda^2} .$$

The boundary conditions at $z = L$ require:

$$\begin{aligned} \hat{z}_x \bar{\bar{G}}_4^{(11)} &= \hat{z}_x \bar{\bar{G}}_4^{(21)} \Big|_{z=L} \\ \frac{1}{\epsilon_1} \hat{z}_x \nabla_x \bar{\bar{G}}_4^{(11)} &= \frac{1}{\epsilon_2} \hat{z}_x \nabla_x \bar{\bar{G}}_4^{(21)} \Big|_{z=L} \end{aligned}$$

Substituting (2.13) into these equations we obtain:

$$\begin{aligned} e^{ihL} + S_m \left[e^{-ihL} + e^{ihL} \right] &= P_m e^{ih_E L} \\ \frac{h}{k} e^{ihL} + S_e \left[-\frac{h}{k} e^{-ihL} - \frac{h}{k} e^{ihL} \right] &= P_e \frac{h_E}{k_E} e^{ih_E L} \\ \frac{h}{\epsilon_1} e^{ihL} + S_m \left[-\frac{h}{\epsilon_1} e^{-ihL} + \frac{h}{\epsilon_1} e^{ihL} \right] &= P_m \frac{h_E}{\epsilon_2} e^{ih_E L} \\ \frac{k}{\epsilon_1} e^{ihL} + S_e \left[\frac{k}{\epsilon_1} e^{-ihL} - \frac{k}{\epsilon_1} e^{ihL} \right] &= \frac{k_E}{\epsilon_2} P_e e^{ih_E L} . \end{aligned}$$

Hence:

$$S_m = \frac{(h_E - n^2 h) e^{ihL}}{2 \left[n^2 h \sin(hL) - h_E \cos(hL) \right]} \quad (2.14)$$

$$P_m = \frac{n^2 h e^{-ih_E L}}{h_E \cos(hL) - n^2 h \sin(hL)} \quad (2.15)$$

$$S_e = \frac{(h - h_E) e^{ihL}}{2[h \cos(hL) - i h_E \sin(hL)]} \quad (2.16)$$

$$P_e = \frac{nh e^{-ih_E L}}{[h \cos(hL) - i h_E \sin(hL)]} \quad (2.17)$$

where $n^2 = \epsilon_2/\epsilon_1$.

Thus, knowing the expression for $\bar{G}_4^{(11)}$, an application of Green's identity gives an integral form of the magnetic field due a constant current loop distribution

$$\bar{H}(\bar{R}) = k^2 \iiint \bar{G}_4^{(11)} \cdot \bar{m}(\bar{R}') dV' \quad L > z > 0 ,$$

$$\bar{H}(\bar{R}) = n^2 k^2 \iiint \bar{G}_4^{(21)} \cdot \bar{m}(\bar{R}') dV' \quad z > L .$$

2.5 Symmetry Property of Dyadic Green's Function

Analogous to the scalar Green's functions, the dyadic Green's functions have certain symmetry properties which are described in detail by Tai [6]. In his book, only problems involving two media have been discussed. It is not difficult to extend the multi-media problems. In this section, we extend one of Tai's relationships to a two layer problem.

Let us consider the problem in our research. The functions $\bar{G}_3^{(11)}$, $\bar{G}_3^{(21)}$, $\bar{G}_4^{(11)}$ and $\bar{G}_4^{(21)}$ satisfy the following equations:

$$\nabla_x \nabla_x \bar{G}_3^{(11)}(\bar{R}/\bar{R}_a) - k_E^2 \bar{G}_3^{(11)}(\bar{R}/\bar{R}_a) = \bar{I} \delta(\bar{R} - \bar{R}_a)$$

$$\nabla_x \nabla_x \bar{G}_3^{(21)}(\bar{R}/\bar{R}_a) - k_E^2 \bar{G}_3^{(21)}(\bar{R}/\bar{R}_a) = 0$$

$$\nabla_x \nabla_x \bar{G}_4^{(11)}(\bar{R}/\bar{R}_b) - k_E^2 \bar{G}_4^{(11)}(\bar{R}/\bar{R}_b) = \bar{I} \delta(\bar{R} - \bar{R}_b)$$

$$\nabla \times \nabla \times \bar{\bar{G}}_4^{(21)}(\bar{R}/\bar{R}_b) - k_E^2 \bar{\bar{G}}_4^{(21)}(\bar{R}/\bar{R}_b) = 0$$

where \bar{R}_a and \bar{R}_b are assumed to be in region 1. At the interface $z = L$, these functions satisfy the boundary conditions that

$$\begin{aligned} \hat{n} \times \bar{\bar{G}}_3^{(11)} &= \hat{n} \times \bar{\bar{G}}_3^{(21)} \\ \frac{-1}{\mu_1} \hat{n} \times \nabla \times \bar{\bar{G}}_3^{(11)} &= \frac{1}{\mu_2} \hat{n} \times \nabla \times \bar{\bar{G}}_3^{(21)} \\ \hat{n} \times \bar{\bar{G}}_4^{(11)} &= \hat{n} \times \bar{\bar{G}}_4^{(21)} \\ \frac{1}{\epsilon_1} \hat{n} \times \nabla \times \bar{\bar{G}}_4^{(11)} &= \frac{1}{\epsilon_2} \hat{n} \times \nabla \times \bar{\bar{G}}_4^{(21)} \end{aligned} \quad (2.18)$$

The vector Green's first identity has the form

$$\iiint_V \left[(\nabla \times \bar{P}) \cdot (\nabla \times \bar{Q}) - \bar{Q} \cdot \nabla \times \nabla \times \bar{P} \right] dV = \iint_S (\bar{Q} \times \nabla \times \bar{P}) \cdot d\bar{S} .$$

We form two vector functions defined by

$$\bar{P}_1 = \bar{\bar{G}}_4^{(11)}(\bar{R}/\bar{R}_b) \cdot \bar{b} ,$$

$$\bar{Q}_1 = \nabla \times \bar{\bar{G}}_3^{(11)}(\bar{R}/\bar{R}_a) \cdot \bar{a} .$$

An application of the Green's first identity in region 1 yields:

$$\begin{aligned} &\underbrace{\bar{b} \cdot \nabla \times \bar{\bar{G}}_4^{(11)}(\bar{R}_a/\bar{R}_b) \cdot \bar{a}}_{-} - \underbrace{\bar{a} \cdot \nabla \times \bar{\bar{G}}_3^{(11)}(\bar{R}_b/\bar{R}_a) \cdot \bar{b}}_{+} + \\ &+ \iiint_V k^2 \left\{ \left[\nabla \times \bar{\bar{G}}_4^{(11)}(\bar{R}/\bar{R}_b) \cdot \bar{b} \right] \cdot \left[\bar{\bar{G}}_3^{(11)}(\bar{R}/\bar{R}_a) \cdot \bar{a} \right] - \left[\nabla \times \bar{\bar{G}}_3^{(11)}(\bar{R}/\bar{R}_a) \cdot \bar{a} \right] \cdot \left[\bar{\bar{G}}_4^{(11)}(\bar{R}/\bar{R}_b) \cdot \bar{b} \right] \right\} dV = \end{aligned}$$

$$= \iint_{S_1} \left[\nabla \times \bar{\bar{G}}_3^{(11)}(\bar{R}/\bar{R}_a) \cdot \bar{a} \times \nabla \times \bar{\bar{G}}_4^{(11)}(\bar{R}/\bar{R}_b) \cdot \bar{b} \right] \cdot d\bar{S}$$

where \sim as before means the transpose of the dyad.

The volume integral in the above equation can be changed into a surface integral by means of Gauss' theorem since it is equal to

$$k^2 \iiint \nabla \cdot \left\{ \left[\bar{\bar{G}}_4^{(11)}(\bar{R}/\bar{R}_b) \cdot \bar{b} \right] \times \left[\bar{\bar{G}}_3^{(11)}(\bar{R}/\bar{R}_a) \cdot \bar{a} \right] \right\} dV .$$

As a result of the radiation condition and the boundary condition at the perfectly conducting plane, the resultant surface integral exists only on the interface S_L . Thus, we have

$$\begin{aligned} & \bar{b} \cdot \underbrace{\nabla \times \bar{\bar{G}}_4^{(11)}(\bar{R}_a/\bar{R}_b)}_{\sim} \cdot \bar{a} - \bar{a} \cdot \underbrace{\nabla \times \bar{\bar{G}}_3^{(11)}(\bar{R}_b/\bar{R}_a)}_{\sim} \cdot \bar{b} = \\ & = -k^2 \iint_{S_L} \left\{ \left[\bar{\bar{G}}_4^{(11)}(\bar{R}/\bar{R}_b) \cdot \bar{b} \right] \times \left[\bar{\bar{G}}_3^{(11)}(\bar{R}/\bar{R}_a) \cdot \bar{a} \right] \right\} \cdot d\bar{S} + \\ & + \iint_{S_L} \left[\nabla \times \bar{\bar{G}}_3^{(11)}(\bar{R}/\bar{R}_a) \cdot \bar{a} \times \nabla \times \bar{\bar{G}}_4^{(11)}(\bar{R}/\bar{R}_b) \cdot \bar{b} \right] \cdot d\bar{S} . \end{aligned} \quad (2.19)$$

Similarly, by letting

$$\bar{P}_2 = \bar{\bar{G}}_4^{(21)}(\bar{R}/\bar{R}_b) \cdot \bar{b}$$

$$\bar{Q}_2 = \nabla \times \bar{\bar{G}}_3^{(21)}(\bar{R}/\bar{R}_a) \cdot a$$

and applying Green's first identity to region 2 covering the entire domain $z \geq L$, we obtain

$$\begin{aligned}
& \iiint \left\{ \left[\nabla_x \bar{\bar{G}}_4^{(21)}(\bar{R}/\bar{R}_b) \cdot \bar{b} \right] \cdot \left[k_E^2 \bar{\bar{G}}_3^{(21)}(\bar{R}/\bar{R}_a) \cdot \bar{a} \right] - \left[\nabla_x \bar{\bar{G}}_3^{(21)}(\bar{R}/\bar{R}_a) \cdot \bar{a} \right] \cdot \left[k_E^2 \bar{\bar{G}}_4^{(21)}(\bar{R}/\bar{R}_b) \cdot \bar{b} \right] \right\} dV = \\
& = \iint_{S_2} \left[\nabla_x \bar{\bar{G}}_3^{(21)}(\bar{R}/\bar{R}_a) \cdot \bar{a} \times \nabla_x \bar{\bar{G}}_4^{(21)}(\bar{R}/\bar{R}_b) \cdot \bar{b} \right] \cdot d\bar{S} .
\end{aligned}$$

As a result of the application of Gauss' theorem to the volume integral and the radiation condition at infinity, the only surface integral left is on the interface S_L . Thus:

$$\begin{aligned}
& k_E^2 \iint_{S_L} \left[\bar{\bar{G}}_4^{(21)}(\bar{R}/\bar{R}_b) \cdot \bar{b} \right] \times \left[\bar{\bar{G}}_3^{(21)}(\bar{R}/\bar{R}_a) \cdot \bar{a} \right] \cdot d\bar{S} = \\
& = \iint_{S_L} \left[\nabla_x \bar{\bar{G}}_3^{(21)}(\bar{R}/\bar{R}_a) \cdot \bar{a} \times \nabla_x \bar{\bar{G}}_4^{(21)}(\bar{R}/\bar{R}_b) \cdot \bar{b} \right] \cdot d\bar{S} . \quad (2.20)
\end{aligned}$$

In view of Eqs. (2.19) and (2.20) and noticing that $k_E^2 = n^2 k^2$, we have

$$\begin{aligned}
& \bar{b} \cdot \nabla_x \bar{\bar{G}}_4^{(11)}(\bar{R}_a/\bar{R}_b) \cdot \bar{a} - \bar{a} \cdot \nabla_x \bar{\bar{G}}_3^{(11)}(\bar{R}_b/\bar{R}_a) \cdot \bar{b} \\
& = -k^2 \iint_{S_L} \left\{ \left[\bar{\bar{G}}_4^{(11)}(\bar{R}/\bar{R}_b) \cdot \bar{b} \right] \times \left[\bar{\bar{G}}_3^{(11)}(\bar{R}/\bar{R}_a) \cdot \bar{a} \right] \right\} \cdot d\bar{S} - \\
& + k^2 \iint_{S_L} \left\{ \left[\bar{\bar{G}}_4^{(21)}(\bar{R}/\bar{R}_b) \cdot \bar{b} \right] \times \left[\bar{\bar{G}}_3^{(21)}(\bar{R}/\bar{R}_a) \cdot \bar{a} \right] \right\} \cdot d\bar{S} \\
& + \iint_{S_L} \left[\nabla_x \bar{\bar{G}}_3^{(11)}(\bar{R}/\bar{R}_a) \cdot \bar{a} \right] \times \left[\nabla_x \bar{\bar{G}}_4^{(11)}(\bar{R}/\bar{R}_b) \cdot \bar{b} \right] \cdot d\bar{S}
\end{aligned}$$

$$-\frac{1}{n^2} \iint_{S_L} \left[\nabla_x \bar{\bar{G}}_3^{(21)}(\bar{R}/\bar{R}_a) \cdot \bar{a} \right] x \left[\nabla_x \bar{\bar{G}}_4^{(21)}(\bar{R}/\bar{R}_b) \cdot \bar{b} \right] \cdot d\bar{S} .$$

When the boundary conditions (2.18) are applied, the surface integral over the interface S_L vanishes. Thus

$$\bar{b} \cdot \nabla_x \bar{\bar{G}}_4^{(11)}(\bar{R}_a/\bar{R}_b) \cdot \bar{a} = \bar{a} \cdot \nabla_x \bar{\bar{G}}_3^{(11)}(\bar{R}_b/\bar{R}_a) \cdot \bar{b} .$$

Putting $\nabla_x \bar{\bar{G}}_3^{(11)}(\bar{R}_b/\bar{R}_a) = \bar{A} \bar{B}$, gives

$$\begin{aligned} \bar{a} \cdot \nabla_x \bar{\bar{G}}_3^{(11)}(\bar{R}_b/\bar{R}_a) \cdot \bar{b} &= \bar{a} \cdot (\bar{B} \bar{A}) \cdot \bar{b} = (\bar{a} \cdot \bar{B})(\bar{A} \cdot \bar{b}) \\ &= (\bar{b} \cdot \bar{A})(\bar{B} \cdot \bar{a}) = \bar{b} \cdot (\bar{A} \bar{B}) \cdot \bar{a} \\ &= \bar{b} \cdot \nabla_x \bar{\bar{G}}_3^{(11)}(\bar{R}_b/\bar{R}_a) \cdot \bar{a} . \end{aligned}$$

Since \bar{a} and \bar{b} are arbitrary constant vectors,

$$\nabla_x \bar{\bar{G}}_4^{(11)}(\bar{R}_a/\bar{R}_b) = \nabla_x \bar{\bar{G}}_3^{(11)}(\bar{R}_b/\bar{R}_a) .$$

Replacing \bar{R}_a by \bar{R}' and \bar{R}_b by \bar{R} , we obtain

$$\tilde{\nabla}'_x \bar{\bar{G}}_4^{(11)}(\bar{R}'/\bar{R}) = \nabla_x \bar{\bar{G}}_3^{(11)}(\bar{R}/\bar{R}') . \quad (2.21)$$

Here the \sim covers the whole dyadic function according to Tai's notation.

In examining the multi-reflection coefficients R_m , R_e , S_m and S_e , it is found that the following relationships exist:

$$S_m = R_m , \quad S_e = R_e .$$

Thus, the $\bar{\bar{G}}_3$ and $\bar{\bar{G}}_4$ functions derived for our problem have the symmetry

property as is clearly seen in Eq. (2.21). This procedure could easily be extended to other multi-media problems.

2.6 Impedance Boundary Condition

During the early 1940's, a large number of Russian papers were published dealing with various aspects of wave propagation over the earth. An attempt was made to take into account the actual properties of ground materials by specifying an impedance boundary condition at the surface. These conditions are

attributed to Leontovich (for example, see Fock [12]) and were described to Leontovich [13]. Application of these boundary conditions to propagation problems has been discussed by Feynberg [14]. A straightforward and comprehensive study was done by Hiatt et al [15]; they obtained the following results

when $|n| \gg 1$:

$$\frac{\partial E_z}{\partial z} = -\frac{ik}{n} E_z \Big|_{z=0}$$

$$\frac{\partial H_z}{\partial z} = -ikn H_z \Big|_{z=0}$$

where the interface is located at $z = 0$ and the positive z direction is upward toward the free space.

2.7 Approximate Dyadic Green's Function Satisfying the Impedance Boundary Condition

Analytically, when the impedance boundary condition is used, the formulation becomes different from the one presented in previous sections. The impedance boundary conditions at the interface $z = L$ imply that there is no wave propagating beyond the interface. The method of obtaining the Green's function remains the same. Using the dyadic Green's function of the first kind as the basis and applying scattering superposition technique, we obtain

$$\bar{\bar{G}}_{3I} = \frac{i}{4\pi} \int_0^\infty \frac{d\lambda}{\lambda} \sum_{n=0}^{\infty} \frac{2^{-\delta_0}}{h} \left\{ \begin{aligned} & \bar{M}(h) \left[\bar{M}'(-h) - \bar{M}'(h) \right] + \bar{N}(h) \left[\bar{N}'(-h) + \bar{N}'(h) \right] + \\ & \left[\bar{M}(-h) - \bar{M}(h) \right] \bar{M}'(h) + \left[\bar{N}(-h) + \bar{N}(h) \right] \bar{N}'(h) + \end{aligned} \right.$$

$$\left. \begin{aligned}
 & + R_{eI} \left[\bar{M}(-h) - \bar{M}(h) \right] \left[\bar{M}'(-h) - \bar{M}'(h) \right] + R_{mI} \left[\bar{N}(-h) + \bar{N}(h) \right] \left[\bar{N}'(-h) + \bar{N}'(h) \right] \\
 & + R_{eI} \left[\bar{M}(-h) - \bar{M}(h) \right] \left[\bar{M}'(-h) - \bar{M}'(h) \right] + R_{mI} \left[\bar{N}(-h) + \bar{N}(h) \right] \left[\bar{N}'(-h) + \bar{N}'(h) \right]
 \end{aligned} \right\} \begin{array}{l} L \geq z > z' \\ z' > z \geq 0 \end{array} \quad (2.22)$$

where R_{eI} and R_{mI} are unknown coefficients and the subscript I is used to denote the modified coefficients under the impedance boundary condition.

The Leontovich boundary conditions mentioned before correspond, at $z = L$, to

$$-\frac{\partial E_z}{\partial z} + \frac{ik}{n} E_z = 0$$

$$-\frac{\partial H_z}{\partial z} + ik n H_z = 0 .$$

Under the assumption that $\mu_0 = \mu_1 = \mu_2$, the impedance boundary conditions in dyadic form are:

$$\left. \begin{aligned}
 & \hat{z} \cdot \left(-\frac{\partial \bar{G}_{3I}}{\partial z} + \frac{ik}{n} \bar{G}_{3I} \right) = 0 \\
 & \hat{z} \cdot \left(-\frac{\partial}{\partial z} \nabla_x \bar{G}_{3I} + ik n \nabla_x \bar{G}_{3I} \right) = 0
 \end{aligned} \right|_{z=L} . \quad (2.23)$$

Substituting Eq. (2.2) and (2.22) into (2.23) yields:

$$\begin{aligned}
 & -ihe^{ihL} + R_{mI} (ihe^{-ihL} - ihe^{ihL}) + \frac{ik}{n} \left[e^{ihL} + R_{mI} (e^{-ihL} + e^{ihL}) \right] = 0 , \\
 & -ihe^{ihL} + R_{eI} (ihe^{-ihL} + ihe^{ihL}) + ikn \left[e^{ihL} + R_{eI} (e^{-ihL} - e^{ihL}) \right] = 0 .
 \end{aligned}$$

Hence,

$$R_{mI} = \frac{e^{ihL}(k-nh)}{2 \left[nh \sin(hL) - k \cos(hL) \right]} \quad (2.24)$$

$$R_{eI} = \frac{e^{ihL}(nk - h)}{2[ikn \sin(hL) - h \cos(hL)]} . \quad (2.25)$$

The same procedure carries over for \bar{G}_{4I} . It yields:

$$\begin{aligned} \bar{\bar{G}}_{4I} = & \frac{i}{4\pi} \int_0^\infty \frac{d\lambda}{\lambda} \sum_{n=0}^{\infty} \frac{2-\delta}{h} \left\{ \begin{array}{l} \bar{M}(h) [\bar{M}'(-h) + \bar{M}'(h)] + \bar{N}(h) [\bar{N}'(-h) - \bar{N}'(h)] + \\ [\bar{M}(-h) + \bar{M}(h)] \bar{M}'(h) + [\bar{N}(-h) - \bar{N}(h)] \bar{N}'(h) + \\ + S_{mI} [\bar{M}(-h) + \bar{M}(h)] [\bar{M}'(-h) + \bar{M}'(h)] + S_{eI} [\bar{N}(-h) - \bar{N}(h)] [\bar{N}'(-h) - \bar{N}'(h)] \\ + S_{mI} [\bar{M}(-h) + \bar{M}(h)] [\bar{M}'(-h) + \bar{M}'(h)] + S_{eI} [\bar{N}(-h) - \bar{N}(h)] [\bar{N}'(-h) - \bar{N}'(h)] \end{array} \right\} \begin{array}{l} L \geq z > z' \\ z' > z \geq 0 \end{array} \end{aligned} \quad (2.26)$$

The impedance boundary conditions at $z = L$ are:

$$\hat{z} \cdot \left(-\frac{\partial \bar{\bar{G}}_{4I}}{\partial z} + i kn \bar{\bar{G}}_{4I} \right) = 0 \Big|_{z=L} \quad (2.27)$$

$$\frac{1}{\epsilon_1} \hat{z} \cdot \left(-\frac{\partial}{\partial z} \nabla_x \bar{\bar{G}}_{4I} + \frac{ik}{n} \nabla_x \bar{\bar{G}}_{4I} \right) = 0 \Big|_{z=L} . \quad (2.28)$$

Substituting Eq. (2.2) and (2.26) into (2.27) and (2.28) we obtain

$$\begin{aligned} -ihe^{ihL} + S_{eI} \left[ihe^{-ihL} + ihe^{ihL} \right] + ikn \left[e^{ihL} + S_{eI} (e^{-ihL} - e^{ihL}) \right] &= 0 , \\ -ihe^{ihL} + S_{mI} \left[ihe^{-ihL} - ihe^{ihL} \right] + \frac{ik}{n} \left[e^{ihL} + S_{mI} (e^{-ihL} + e^{ihL}) \right] &= 0 . \end{aligned}$$

The above two equations can be solved for the two unknowns:

$$S_{eI} = \frac{(h - kn) e^{ihL}}{2[h \cos(hL) - i kn \sin(hL)]} \quad (2.29)$$

$$S_{mI} = \frac{(nh - k) e^{ihL}}{2[k \cos(hL) - i hn \sin(hL)]} . \quad (2.30)$$

Thus we have obtained the expressions for two approximate dyadic Green's functions by applying the Leontovich impedance boundary condition to one problem.

2.8 Relationship Between Exact and Approximate Green's Function

The difference between the exact Green's function and the approximate Green's function is that the former uses the continuous property of electric and magnetic fields at interfaces while the latter imposes the Leontovich boundary conditions at interfaces. Thus, the structure of Eqs. (2.5) and (2.22) is identical with the exception that the multiple reflection coefficients are different.

To determine how close the Leontovich boundary condition approximates the exact boundary condition, it is necessary to study the physical meaning of the impedance condition. The fact that such an impedance exists at the interface between two medium can be clearly seen by considering a plane wave incident on the boundary from the direction of free space. Application of Snell's law shows that the transmitted wave is deflected toward the normal because of the refractive index n . For a fixed direction of incidence, the angle between the direction of the transmitted field and the normal of the interface is in the order of $\frac{1}{|n|}$, which implies that the radial eigenvalue λ of the transmitted field is in the order of $\sin(\frac{1}{|n|})$. For a value of the refractive index $|n|$ large compared to unity, the eigenvalue λ is negligible. Thus

$$h_E \approx k_E = nk \quad (2.31)$$

The same relationship holds in our problem. When the approximation $h_E \approx nk$ is put into R_e and R_m , simple algebraic manipulation gives rise to the expressions for R_{eI} and R_{mI} . Similar arguments hold for the relationship between S_e , S_m and S_{eI} , S_{mI} . Thus, it is clearly seen that the larger the value of n , the closer the two solutions. In other words, when the refractive index is in the order of unity it is not suitable to use impedance boundary condition.

CHAPTER III

FIELDS DUE TO HERTZIAN DIPOLES

3.1 Introduction

The dyadic Green's functions needed in our problem have been given explicitly in Chapter II. These Green's functions can be used to find an integral form for the fields in the region in between two interfaces for any kind of current source. In general, any current source can be decomposed into elementary Hertzian dipoles. So only the fields due to x-directed and z-directed Hertzian electric and magnetic dipoles are considered.

In general, the exact form of the field is rather difficult to find. However, an asymptotic solution can be found using saddle point integration which has been discussed in great detail by many authors [13], [14].

3.2 z-directed Dipole

3.2.1 Integral Representation

For a z-directed infinitesimal electric dipole located at a height z_0 above the interface $z = 0$, the current distribution can be expressed as

$$\bar{J}(\bar{R}') = \hat{z} \delta(x' - 0) \delta(y' - 0) \delta(z' - z_0) I\ell . \quad (3.1)$$

The antenna current distribution is assumed to be uniform with a magnitude I . If the length of the antenna is ℓ then in the limit as ℓ goes to zero, the current I goes to infinity and the dipole moment $I\ell$ is assumed to have a finite value. Since the Green's functions derived before contain posterior terms of the

$\bar{M}'_{e n \lambda}^{(\pm h)}$ and $\bar{N}'_{e n \lambda}^{(\pm h)}$, the following two relationships, which arise from the explicit expressions for the M and N functions given in Eq. (2.2), enable us to write:

$$\begin{aligned} \iiint \bar{M}'_{e n \lambda}^{(\pm h)} \cdot \bar{J}(\bar{R}') dV' &= 0 \\ \iiint \bar{N}'_{e n \lambda}^{(\pm h)} \cdot \bar{J}(\bar{R}') dV' &= I\ell \frac{\delta_0^2}{k} e^{\pm i h z_0} . \end{aligned} \quad (3.2)$$

Equation (3.2) implies that the final expression for \bar{E} will contain only terms of $\bar{N}_{e0\lambda}$ type, because the \bar{M} functions have no z component.

We recall that the electric field may be found from a knowledge of the current distribution and the Green's function. The specific relationship is:

$$\bar{E} = i\omega\mu_0 \iiint \bar{G}(\bar{R}/\bar{R}') \cdot \bar{J}(\bar{R}') dV' .$$

Substituting Eq. (3.2) into the above equation, we obtain

$$\begin{aligned} \bar{E} = -\frac{\omega\mu_0 I \ell}{4\pi k} \int_0^\infty \frac{\lambda d\lambda}{h} & \left\{ \begin{array}{l} \bar{N}_{e0\lambda}(h) \left[e^{-ihz_o} + e^{ihz_o} \right] + \\ \left[\bar{N}_{e0\lambda}(-h) + \bar{N}_{e0\lambda}(h) \right] e^{ihz_o} + \\ + R_m \left[\bar{N}_{e0\lambda}(-h) + \bar{N}_{e0\lambda}(h) \right] \left[e^{-ihz_o} + e^{ihz_o} \right] \end{array} \right\} L \geq z > z_o \\ & + R_m \left[\bar{N}_{e0\lambda}(-h) + \bar{N}_{e0\lambda}(h) \right] \left[e^{-ihz_o} + e^{ihz_o} \right] \left\{ \begin{array}{l} z_o > z \geq 0 \end{array} \right. \end{aligned} \quad (3.3)$$

The electric field representation is in the form of a semi-infinite integral. Under certain conditions to be stated later, we can find the asymptotic expression by the method of saddle point integration. To derive this expression we shall first transform the integral as given by (3.3) from semi-infinite path to an infinite path in the λ -plane. Applying Sommerfeld's half-circuit relation [16] between the two kinds of Hankel functions and the circulation relation of Hankel functions:

$$J_0(\lambda r) = \frac{1}{2} \left\{ H_0^{(1)}(\lambda r) + H_0^{(2)}(\lambda r) \right\}$$

$$H_0^{(2)}(\lambda r) = -H_0^{(1)}(-\lambda r)$$

to our integral, we obtain

$$\bar{E} = -\frac{\omega \mu_0 I \ell}{4\pi k} \int_{-\infty}^{\infty} \frac{\lambda d\lambda}{h} \left\{ \begin{array}{l} \bar{N}_{e0\lambda}^{(1)}(h) 2 \cos(hz_o) + R_m \left[\bar{N}_{e0\lambda}^{(1)}(-h) + \bar{N}_{e0\lambda}^{(1)}(h) \right] 2 \cos(hz_o) \\ \left[\bar{N}_{e0\lambda}^{(1)}(-h) + \bar{N}_{e0\lambda}^{(1)}(h) \right] e^{ihz_o} + R_m \left[\bar{N}_{e0\lambda}^{(1)}(-h) + \bar{N}_{e0\lambda}^{(1)}(h) \right] 2 \cos(hz_o) \end{array} \right\} \quad (3.4)$$

where

$$\bar{N}_{e0\lambda}^{(1)}(\pm h) = \nabla \times \left[H_0^{(1)}(\lambda r) e^{\pm i h z} \hat{z} \right].$$

This is the exact integral representation of the electric field due to a z-directed infinitesimal electric dipole. The final task is to evaluate this integral.

3.2.2 Asymptotic Solution

When λr is large compared to unity, corresponding to a far-zone field, the Hankel function in $\bar{M}^{(1)}$ and $\bar{N}^{(1)}$ can be approximated by its asymptotic expansion

$$H_n^{(1)}(\eta r) \approx \sqrt{\frac{2}{\pi \eta r}} (-i)^{n+1/2} e^{i \eta r}.$$

Accordingly, the functions $\bar{M}^{(1)}$ and $\bar{N}^{(1)}$ become:

$$\bar{M}_{e n \eta}^{(1)}(\pm h) \approx (-i)^{n+3/2} \eta \sqrt{\frac{2}{\pi \eta r}} e^{i(\eta r \pm hz)} \frac{\cos n\phi}{\sin n\phi},$$

$$\bar{N}_{e n \eta}^{(1)}(\pm h) \approx (-i)^{n+1/2} \eta \sqrt{\frac{2}{\pi \eta r}} e^{i(\eta r \pm hz)} \frac{\cos n\phi}{\sin n\phi} \left[\frac{(\mp h\hat{r} + n\hat{z})}{k} \right].$$

Then, the far-zone electric field is represented by:

$$\bar{E} \approx \left\{ \begin{array}{l} -\frac{\omega \mu_0 I \ell}{4\pi k} \int_{-\infty}^{\infty} \frac{d\lambda}{h} (-i)^{1/2} \lambda^2 \sqrt{\frac{2}{\pi \lambda r}} \left\{ 2 \cos(hz_o) \frac{(\lambda \hat{z} - h\hat{r})}{k} e^{i(\lambda r + hz)} (1 + R_m) + \right. \right. \\ \left. \left. + R_m 2 \cos(hz_o) e^{i(\lambda r - hz)} \frac{(\lambda \hat{z} + h\hat{r})}{k} \right\} \quad L \geq z > z_o \end{array} \right.$$

$$\left\{ -\frac{\omega \mu_0 I t}{4\pi k} \int_{-\infty}^{\infty} \frac{d\lambda}{h} (-i)^{1/2} \lambda^2 \sqrt{\frac{2}{\pi \lambda r}} \left\{ e^{ihz_0} + 2R_m \cos(hz_0) \right\} x \right. \\ \left. x \left[e^{i(\lambda r - hz) \frac{(\lambda \hat{z} + h \hat{r})}{k}} + e^{i(\lambda r + hz) \frac{(\lambda \hat{z} - h \hat{r})}{k}} \right] \right\} z_0 > z \geq 0 \quad (3.5)$$

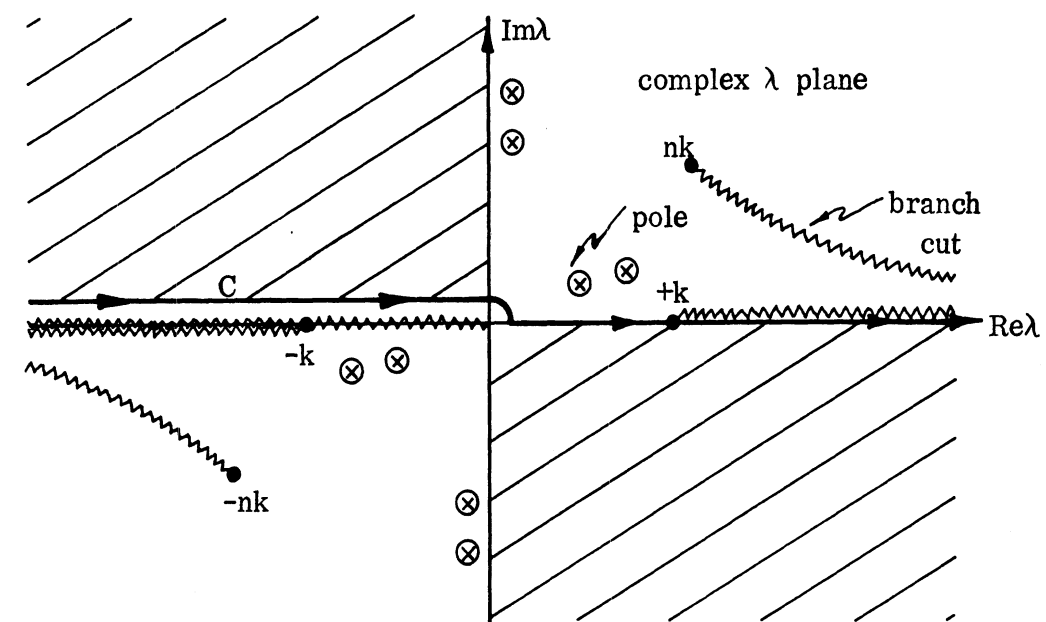
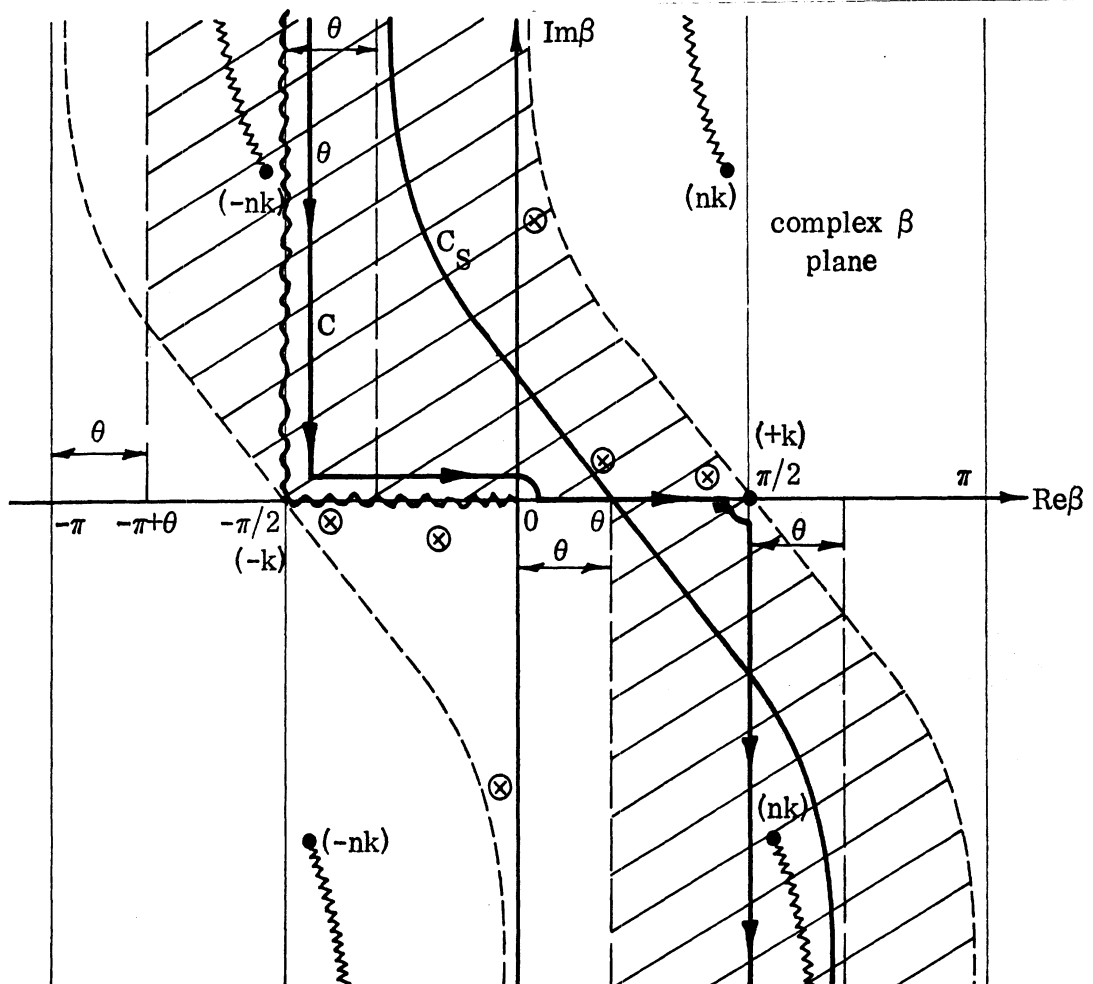
It is desirable to introduce a new complex variable β to execute the integration. This variable is much easier to interpret physically than the eigenvalue λ in the presentation of the wave propagation problem. The technique used here is the same as the one used by Budden [3], Felsen [17] and Nomura [18].

To facilitate the function-theoretic manipulations involving integrals of the type occurring in Eq. (3.5), the new variable β is introduced through the transformation

$$\lambda = k \sin \beta$$

which makes $\lambda = \pm k$ a pair of regular points in the β plane rather than two branch points in the λ plane, since the transcendental function $\sin \beta$ is single valued.

The paths of integration in both complex λ and β planes are shown in Figures 3-1 and 3-2. The reflection coefficient R_m in Eq. (3.5) is a function of $h = \pm \sqrt{k^2 - \lambda^2}$ and $h_E = \pm \sqrt{n^2 k^2 - \lambda^2}$. Corresponding to the four combinations of signs of $\pm \sqrt{k^2 - \lambda^2}$ and $\pm \sqrt{n^2 k^2 - \lambda^2}$, the integrand is four-valued and its Riemann surface has four sheets. These sheets are connected with one another by branch cuts along the line $\text{Re } \sqrt{k^2 - \lambda^2} = 0$ and $\text{Re } \sqrt{n^2 k^2 - \lambda^2} = 0$ from $\lambda = \pm k$ or $\lambda = \pm n k$ to infinity as shown in Fig. 3-1. The choice of branch-cut is discussed in detail in Appendix A. The branch cut starting at the origin is due to the Hankel function of the first kind. Because of this particular choice of branch cut, the diagram of Fig. 3-1 is the upper-most sheet among the four Riemann sheets. It is then defined as $\text{Re } \sqrt{k^2 - \lambda^2} > 0$ and $\text{Re } \sqrt{n^2 k^2 - \lambda^2} > 0$,

FIG. 3-1: PATH OF INTEGRATION IN COMPLEX λ PLANE.FIG. 3-2: PATH OF INTEGRATION IN COMPLEX β PLANE.

where the shaded region represents that imaginary part of the exponential term which is greater than zero. The transformed diagram is shown in Fig. 3-2.

Through the transformation $\lambda = k \sin\beta$, the four Riemann sheets in the λ domain become four adjacent sections in β domain with a period of 2π . The region of concern is that between $-\pi/2$ and $\pi/2$ as shown in Fig. 3-2 which corresponds to the uppermost sheet as shown in Fig. 3-1. The branch cuts starting from $\lambda = \pm k$ in λ domain are shown in dashed lines as regular lines starting from $\beta = \pm\pi/2$ in β domain. Since the integral path C no longer circles around these dashed lines, the introduction of the transformation is now easily realized.

There are poles arising from the denominator of the reflection coefficient R_m . These poles are closely related to the surface wave. A detailed study of the pole characteristic will be given later.

In applying the transformation $\lambda = k \sin \beta$ to Eq. (3.5) the counter transformation pair $h = \pm k \cos \beta$ exists. The choice of the sign again follows the rule that the integral must be convergent in order to satisfy the radiation condition. For the exponential term in the integrand having $i(\lambda r + hz)$ the positive sign has to be chosen, while for $i(\lambda r - hz)$, the negative sign has to be used. Thus, the integral in the complex β domain becomes

$$\begin{aligned}
 E_{(z)} &= \left\{ -\frac{\omega \mu_0 I l}{4\pi k} \int_{-\frac{\pi}{2}-i\infty}^{\frac{\pi}{2}-i\infty} d\beta k^2 \sin^2 \beta \sqrt{\frac{-2i}{\pi R \sin \theta}} \left\{ 2 \cos(kz_0 \cos \beta) (\sin \beta \hat{z} - \cos \beta \hat{r}) (1 + R_m) - \right. \right. \\
 &\quad \left. \left. - R_m^2 \cos(-kz_0 \cos \beta) (\sin \beta \hat{z} - \cos \beta \hat{r}) \right\} e^{ikR \cos(\theta - \beta)} \right. \\
 &\quad \left. L \geq z > z_0 \right. \\
 &= \left\{ -\frac{\omega \mu_0 I l}{4\pi k} \int_{-\frac{\pi}{2}-i\infty}^{\frac{\pi}{2}-i\infty} d\beta k^2 \sin^2 \beta \sqrt{\frac{-2i}{\pi R \sin \theta}} \left\{ - \left[e^{-ikz_0 \cos \beta} + 2R_m \cos(kz_0 \cos \beta) \right] \cdot \right. \right. \\
 &\quad \left. \left. (\sin \beta \hat{z} - \cos \beta \hat{r}) + \left[e^{ikz_0 \cos \beta} + 2R_m \cos(+kz_0 \cos \beta) \right] (\sin \beta \hat{z} - \cos \beta \hat{r}) \right\} e^{ikR \cos(\theta - \beta)} \right. \\
 &\quad \left. z_0 > z \geq 0 \right. \\
 \end{aligned} \tag{3.6}$$

Now the saddle point method is applicable in the complex β plane. The path of steepest descent is shown in Fig. 3-2 as C_S . The deformed path of integration passed over the saddle point at

$$\frac{d}{d\beta} \cos(\theta - \beta) = 0$$

$$\text{where } \theta = \tan^{-1} \frac{r}{z}$$

which gives $\beta = \theta$ as a saddle point.

If the path C_S does not pass near a singularity nor cross singularities when deformed, the asymptotic solution of the integration is

$$\bar{E}_z(z) \approx -\frac{\omega \mu_0 I \ell}{\pi} i \sin \theta \frac{e^{ikR}}{R} \left\{ \cos(kz_0 \cos \theta) (1 + R_m \left|_{k \cos \theta}^{\infty} - R_m \right|_{-k \cos \theta}) x \right. \\ \left. x (\sin \theta \hat{z} - \cos \theta \hat{r}) \right\} \quad L \geq z \geq 0 \quad (3.7)$$

where

$$R_m \left|_{h=\pm k \cos \theta}^{\infty} = \frac{(h k_E^2 - h_E^2)^{1/2} e^{ihL}}{2 \left[k_E^2 h_E^2 \cos(hL) - i k_E^2 h_E \sin(hL) \right]} \right|_{h=\pm k \cos \theta}$$

This is the far-zone electric field solution for the problem of concern. Under our assumption that no singularity is crossed, this far field contains the geometrical optics reflected and direct waves. However, when we deform the path from C to C_S , it is possible that it sweeps through either poles or branch cuts. These singularities contribute the so-called surface waves and lateral waves respectively. They are discussed in more detail in Appendix A.

3.2.3 Comparison with Mode Theory Results

Previously mentioned references [2, 3, 5] approach this waveguide problem using mode theory. Section 3.2.2 mentioned that the poles contribute to the surface wave. Thus, the relationship between the dyadic Green's function

technique and the mode theory approach should be pointed out.

The characteristic equation for the existence of a self-consistent mode in the mode theory is

$$R(\theta) R_E(\theta) \exp(2ikL \cos \theta) = 1 \quad (3.8)$$

where θ is the angle between the plane wave normal and the interface, $R(\theta)$ is the reflection coefficient at one plate $z = 0$, and $R_E(\theta)$ is the reflection coefficient at the other plate $z = L$.

For the TM waves travelling in the waveguide, the Fresnel reflection coefficients at the perfect conductor plate and the earth plate are given by:

$$R(\theta) = 1$$

$$R_E(\theta) = \frac{n^2 \cos \theta - (n^2 - \sin^2 \theta)^{1/2}}{n^2 \cos \theta + (n^2 - \sin^2 \theta)^{1/2}}.$$

Putting the transformation $\lambda = k \sin \theta$, $h = k \cos \theta$ into the above equations and substituting the results into (3.8) yields

$$\frac{n^2 h - (n^2 k^2 - \lambda^2)^{1/2}}{n^2 h + (n^2 k^2 - \lambda^2)^{1/2}} = e^{-2ihL}$$

which is equivalent to

$$\frac{h_E}{n^2 h} = i \tan(hL) \quad (3.9)$$

$$\text{where } h_E = (n^2 k^2 - \lambda^2)^{1/2}.$$

The mode equation (3.9) is identical to the equation of the poles in Eqs. (2.14)

and (2.15).

Similarly, for the TE waves,

$$R(\theta) = -1$$

$$R_E(\theta) = \frac{\cos \theta - (n^2 - \sin^2 \theta)^{1/2}}{\cos \theta + (n^2 - \sin^2 \theta)^{1/2}},$$

and the mode equation can be found as

$$\frac{h}{h_E} = i \tan(hL) . \quad (3.10)$$

This mode condition is identical to the equation of the poles in Eqs. (2.6) and (2.7).

Hence, the poles of the dyadic Green's functions are directly related to waveguide modes. Thus, the discussion of the mode theory only constitutes the pole contribution part of our approach. This important fact implies that when the pole contribution, which is the surface wave, is not dominant among the waves, mode theory alone cannot describe the wave propagation problem completely.

3.2.4 Leontovich Approximate Solution

When the impedance boundary condition is applied at the lossy dielectric surface, the solution is referred to as the approximate solution. As derived previously, the approximate Green's function has the same form as the exact Green's function with the exception that the multi-reflection coefficient has a different value, so the above procedure can be used without change in this section. There is no need to repeat the entire discussion here. The asymptotic solution is as follows:

$$\bar{E}_{(z)I} \approx -\frac{\omega \mu_0 I \ell}{\pi} i \sin \theta \frac{e^{ikR}}{R} \cos(kz_0 \cos \theta) (1 + R_{mI}) \left| \begin{array}{c} -R_{mI} \\ k \cos \theta \\ -k \cos \theta \end{array} \right\rangle x \\ x (\sin \theta \hat{z} - \cos \theta \hat{x}) \quad (3.11)$$

where

$$R_{mI} \left|_{\pm k \cos \theta} \right. = \frac{(k - nh) e^{ihL}}{2 [nh \sin(hL) - k \cos(hL)]} \left|_{\pm k \cos \theta} \right.$$

Again this field contains only the direct and reflected waves defined in geometrical optics.

3.3 x-directed Dipole

3.3.1 Exact Solution

For an x-directed infinitesimal electric dipole with current moment $I\ell$ and placed at $z = z_0$, the current distribution may be written as

$$\bar{J}(\bar{R}') = \hat{x} \delta(x' - 0) \delta(y' - 0) \delta(z' - z_0) I\ell .$$

Then

$$\iiint_{\substack{\bar{M}' \\ 0 \\ e \\ n \\ \lambda}} (\pm h) \cdot \bar{J}(\bar{R}') dV' = I\ell \delta_{nl} \frac{\lambda}{2} e^{\pm i h z_0} \quad \text{odd parts} \quad (3.12)$$

$$\iiint_{\substack{\bar{N}' \\ 0 \\ e \\ n \\ \lambda}} (\pm h) \cdot \bar{J}(\bar{R}') dV' = I\ell \delta_{nl} \frac{\pm i h}{k} \frac{\lambda}{2} e^{\pm i h z_0} \quad \text{even parts}$$

where $\delta_{nl} = \begin{cases} 1 & n = 1 \\ 0 & n \neq 1 \end{cases} .$

The terms involved in the calculation of the field are of the type $\bar{M}_{01\lambda}(\pm h)$ and $\bar{N}_{e1\lambda}(\pm h)$. It implies that for a horizontal dipole, it can no longer represent the electric field with one vector wave function alone. This result agrees with Sommerfeld's derivation [16]. Thus, the electric field due to a horizontal electric dipole is:

$$\left\{ \begin{array}{l}
 E_{(x)} = -\frac{\omega \mu_0 I \ell}{4\pi} \int_0^\infty d\lambda \frac{1}{h} \left\{ \bar{M}_{01\lambda}(h) \left[-2i \sin(hz_0) \right] + R_e \left[\bar{M}_{01\lambda}(-h) - \bar{M}_{01\lambda}(h) \right] \left[-2i \sin(hz_0) \right] \right. \right. \\
 \quad \left. \left. + \frac{ih}{k} \left[\bar{N}_{e1\lambda}(h) \left[2i \sin(hz_0) \right] + R_m \left[\bar{N}_{e1\lambda}(-h) + \bar{N}_{e1\lambda}(h) \right] \left[2i \sin(hz_0) \right] \right] \right\} \\
 \quad L \geq z > z_0 \\
 \\
 \left. \begin{array}{l}
 E_{(x)} = -\frac{\omega \mu_0 I \ell}{4\pi} \int_0^\infty d\lambda \frac{1}{h} \left\{ \left[\bar{M}_{01\lambda}(-h) - \bar{M}_{01\lambda}(h) \right] e^{ihz_0} + R_e \left[\bar{M}_{01\lambda}(-h) - \bar{M}_{01\lambda}(h) \right] \left[-2i \sin(hz_0) \right] \right. \right. \\
 \quad \left. \left. + \frac{ih}{k} \left[\left[\bar{N}_{e1\lambda}(-h) + \bar{N}_{e1\lambda}(h) \right] e^{ihz_0} + R_m \left[\bar{N}_{e1\lambda}(-h) + \bar{N}_{e1\lambda}(h) \right] \left[2i \sin(hz_0) \right] \right] \right\} \\
 \quad z_0 > z \geq 0
 \end{array} \right. \quad (3.13)
 \end{array} \right.$$

where subscript (x) means that the field is due to an x-directed dipole.

The basic structure of Eq. (3.13) is the same as Eq. (3.6), hence the procedure used for the vertical dipole case is applicable to the horizontal dipole case. After the application of half-circuit relationship, the path of integration changes to an infinite path in the λ -plane. Substituting the asymptotic expansion of Hankel function and changing the variable of integration into β we can again apply the saddle point method. Thus, the asymptotic solution for an x-directed dipole is found to be

$$\begin{aligned}
 \bar{E}_{(x)} \approx & \frac{\omega \mu_0 I \ell}{\pi} \frac{e^{ikR}}{R} \left\{ \sin(kz_0 \cos \theta) (1 - R_e \left|_{k \cos \theta} \right. + R_e \left|_{-k \cos \theta} \right.) \sin \theta \hat{\phi} + \right. \\
 & \left. + \cos \theta \cos \theta \sin(kz_0 \cos \theta) (1 + R_m \left|_{k \cos \theta} \right. - R_m \left|_{-k \cos \theta} \right.) (\sin \theta \hat{z} - \cos \theta \hat{r}) \right\} \\
 & L \geq z \geq 0 \quad (3.14)
 \end{aligned}$$

where

$$R_e \left|_{h=\pm k \cos \theta} \right. = \frac{(h-h_E) e^{ihL}}{2[h \cos(hL) - i h_E \sin(hL)]} \Bigg|_{h=\pm k \cos \theta}.$$

3.3.2 Leontovich Approximate Solution

Again, following the previous derivation, it is apparent that with the substitution of R_{eI} and R_{mI} into (3.14), we obtain the approximate solution due to a horizontal dipole:

$$\begin{aligned} \bar{E}_{(x)I} \approx & \frac{\omega \mu_0 I l}{\pi} \frac{e^{ikR}}{R} \left\{ \sin(kz_0 \cos \theta) (1 - R_{eI} \left|_{k \cos \theta} + R_{eI} \left|_{-k \cos \theta} \right. \right) \sin \phi \hat{\phi} + \right. \\ & \left. + \cos \theta \cos \phi \sin(kz_0 \cos \theta) (1 + R_{mI} \left|_{k \cos \theta} - R_{mI} \left|_{-k \cos \theta} \right. \right) (\sin \theta \hat{z} - \cos \theta \hat{r}) \right\} \end{aligned} \quad (3.15)$$

where

$$R_{eI} \left|_{h=\pm k \cos \theta} = \frac{(h-nk) e^{ihL}}{2[h \cos(hL) - i n k \sin(hL)]} \right|_{h=\pm k \cos \theta} .$$

3.4 Horizontal Current Loop

As shown by Stratton [20], a convenient measure of the strength of a loop carrying a uniform current is in terms of the magnetic dipole moment. Hence, a small horizontal current loop carrying a current I with area A located at $(0, 0, z_0)$ can be represented by a magnetic dipole with moment

$$\bar{m}(\bar{R}') = \hat{z} \delta(x' - 0) \delta(y' - 0) \delta(z' - z_0) IA .$$

We recall that the magnetic field can be determined with the aid of the following equation:

$$\bar{H} = k^2 \iiint \bar{G}(\bar{R}/\bar{R}') \cdot \bar{m}(\bar{R}') dV' .$$

The analysis is exactly the same as that for a z -directed electric dipole. With the changing of Green's function and excitation factor in Eq. (3.11) the result is given

$$\overline{H}_h \approx i \frac{IAk}{\pi} \sin \theta \frac{e^{ikR}}{R} \sin(kz_0 \cos \theta) (1 + S_e \left|_{k \cos \theta}^{\infty} - S_e \right|_{-k \cos \theta}) \cdot (\sin \theta \hat{z} - \cos \theta \hat{r}) \quad (3.16)$$

where S_e is represented by Eq. (2.16). The approximate solution is obtained by replacing S_e with S_{eI} in Eq. (2.29).

3.5 Vertical Current Loop

For a small vertical current loop carrying current I with area A located at $(0, 0, z_0)$,

$$\overline{m}(R') = \hat{x} \delta(x' - 0) \delta(y' - 0) \delta(z' - z_0) IA .$$

Thus:

$$\begin{aligned} \overline{H}_V &\approx - \frac{IAk}{\pi} \frac{e^{ikR}}{R} \left\{ \cos(kz_0 \cos \theta) (1 - S_m \left|_{k \cos \theta}^{\infty} + S_m \right|_{-k \cos \theta}) \sin \theta \hat{\phi} + \right. \\ &+ \cos \theta \cos \phi \cos(kz_0 \cos \theta) (1 + S_e \left|_{k \cos \theta}^{\infty} - S_e \right|_{-k \cos \theta}) (\sin \theta \hat{z} - \cos \theta \hat{r}) \left. \right\} \\ &L \geq z \geq 0 \end{aligned} \quad (3.17)$$

where S_m is represented by Eq. (2.14).

The replacing of S_m by S_{mI} gives the approximate solution. Thus, the asymptotic expressions of the fields due to various simple dipoles are derived. The similarity of the fields of the electric and magnetic dipoles was expected because of the duality principle. The fields patterns and the detailed results will be presented in the next chapter.

CHAPTER IV

CALCULATION AND DISCUSSION OF RESULTS

4.1 General Remarks

In this chapter we present a computational study of a particular problem involving the wave propagation above lossy earth. The height L of the particular structure is chosen to be 30 meters. The environment of the ground will vary from good to poor earth. The refractive indices associated with these grounds at different frequencies will be cited later. The results based on the Leontovich impedance boundary condition at the lossy interface are studied. The errors associated with these approximate conditions are calculated. For a given elementary point source, the excitation factor is investigated. The advantages of using the dyadic Green's function approach are discussed.

In the following sections, three different types of curves are presented. They are the reflection coefficient modulus, position of the poles in complex θ domain and the far-field pattern for different earth material and frequencies.

4.2 Percentage Error by Using Impedance Boundary Condition

At the very beginning of Chapter III, the Leontovich impedance boundary condition is discussed. This condition is valid only under the assumption that $|n| \gg 1$. However, no quantitative criterion was set for the values of n . The bound of n can not be ascertained in general, since the exact criterion depends on the geometry and the material constant of the earth. In this section we attempt to find the difference between the approximate solution and the exact solution for different values of n .

Let us assume that σ_E and ϵ_E are independent of frequency. The complex index of refraction n is represented as

$$n^2 = \frac{\epsilon_E}{\epsilon_0} \left\{ 1 + i \frac{\sigma_E}{\omega \epsilon_E} \right\} .$$

In general, σ_E and ϵ_E are functions of the water and the salt contents of the earth. Here we categorized earth into two kinds: good earth and poor earth.

The refractive indices as functions of frequency are given below.

frequency used for calculation	good earth ($\epsilon_r = 10, \sigma_E = 10^{-2} \text{ S/m}$)	poor earth ($\epsilon_r = 4, \sigma_E = 10^{-4} \text{ S/m}$)
f	n^2	n^2
60 KHz	$10 + i3000$	$4 + i30$
600 KHz	$10 + i300$	$4 + i3$
6 MHz	$10 + i30$	$4 + i0.3$

Table 4-1: Refractive Index for Different Frequency

In our problem the difference between the exact and approximate solutions is due to the different values of the multi-reflection coefficient. Since the calculations for different types of sources involve different expressions for the reflections it is therefore suitable to plot and discuss the coefficient modulus first. The coefficients R_m and R_{mI} of Eq. (2.8) and (2.24) which relate to both electric dipoles can be written in the form:

$$R_m = \frac{(n^2 \cos \theta - \sqrt{n^2 - \sin^2 \theta}) e^{ikL \cos \theta}}{2 [\sqrt{n^2 - \sin^2 \theta} \cos(kL \cos \theta) - i n^2 \cos \theta \sin(kL \cos \theta)]},$$

$$R_{mI} = \frac{(n \cos \theta - 1) e^{ikL \cos \theta}}{2 [\cos(kL \cos \theta) - i n^2 \cos \theta \sin(kL \cos \theta)]}.$$

The coefficients R_e and R_{eI} , of Eqs. (2.6) and (2.25), relating to the horizontal electric dipole can be written in the form

$$R_e = \frac{(\cos \theta - \sqrt{n^2 - \sin^2 \theta}) e^{ikL \cos \theta}}{2 [\cos \theta \cos(kL \cos \theta) - i \sqrt{n^2 - \sin^2 \theta} \sin(kL \cos \theta)]},$$

$$R_{eI} = \frac{(\cos \theta - n) e^{ikL \cos \theta}}{2 [\cos \theta \cos(kL \cos \theta) - i n \sin(kL \cos \theta)]}.$$

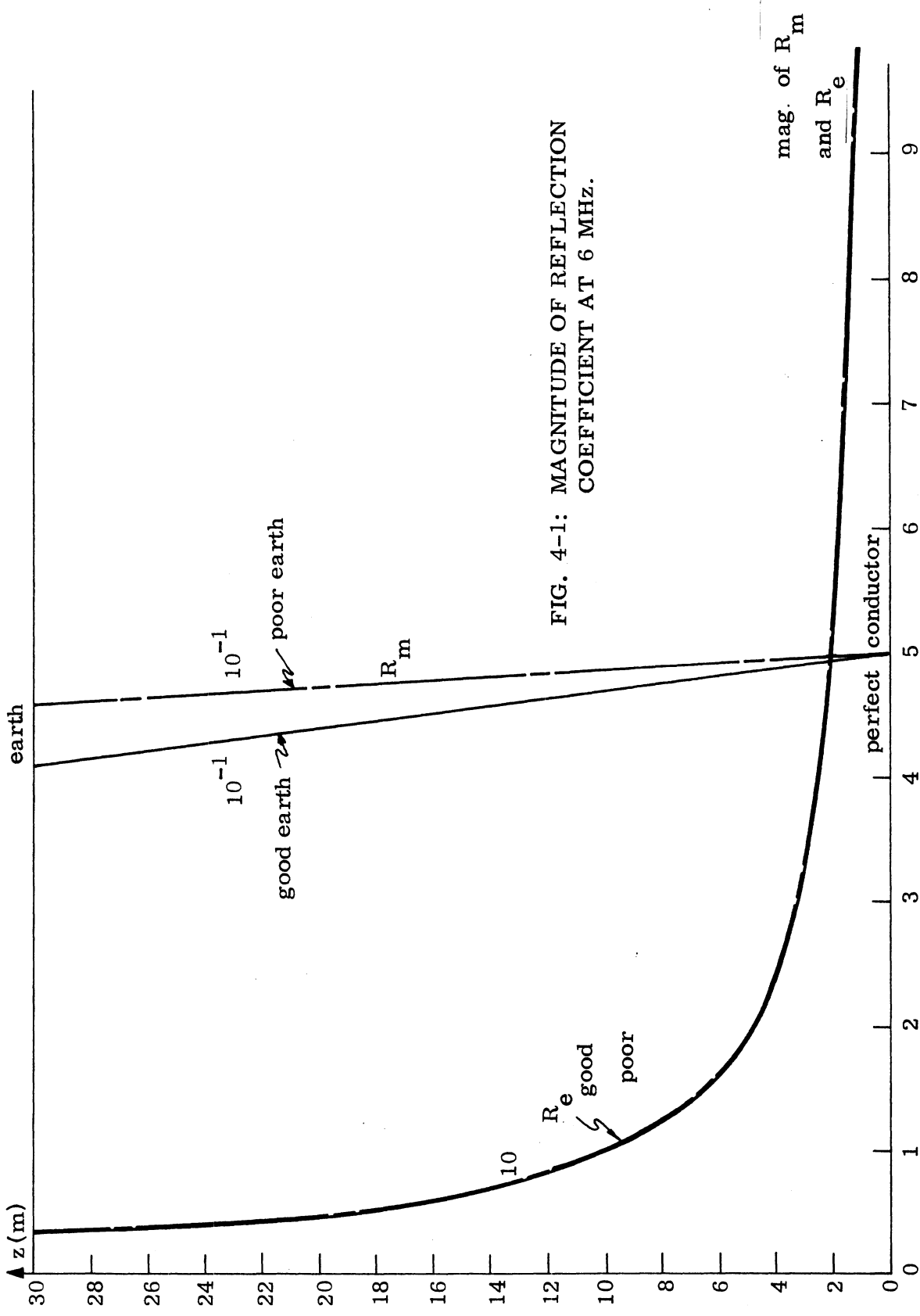
Before showing the curves for the reflection coefficients, it is worthwhile to mention that the cut-off frequency of the guide is 5 MHz, if both plates are perfectly conducting. Thus, 60 KHz is far below this cut-off value. The spatial region of concern is the far zone, thus the direction of observation θ is greater than 82 degrees and less than 90 degrees, hence, the significant range of $\cos \theta$ is extremely small.

Studying Figs. 4-1, 4-2, and 4-3 it is found that the reflection coefficient R_m line gets more perpendicular with both interfaces as the operating frequency gets lower. At low frequencies the earth acts like a perfect conductor implying that the two interfaces look much alike. Thus the R_m curves are more symmetrical with respect to both interfaces. The difference in R_m 's for good earth and poor earth becomes smaller as the frequency is lowered. However, these properties do not apply to R_e . The reason is that there is a pole at $\theta = \pi/2$ as shown in the figures. The difference in the R_e 's gets much larger as the frequency is lowered. Even though the earth surface has a very large refractive index as is the case for $f = 60$ KHz (Fig. 4-3), there is no symmetry property. Thus, the geometry of the structure as well as the nature of the material affects the results.

The following table gives the percentage error in the results when using the impedance boundary condition.

f	n^2	$\cos \theta$	% error of R_{mI}	% error of R_{eI}
6 MHz	$4 + i0.3$	0.039	1.38	0.84
6 MHz	$10 + i30$	0.039	0.35	0.07
600 KHz	$4 + i3$	0.004	0.092	6.925
600 KHz	$10 + i300$	0.004	0.0084	0.016
60 KHz	$4 + i30$	0.0004	0.002	0.358
60 KHz	$10 + i3000$	0.0004	0.0	0.0041

Table 4-2: Percentage Error of Reflection Coefficients



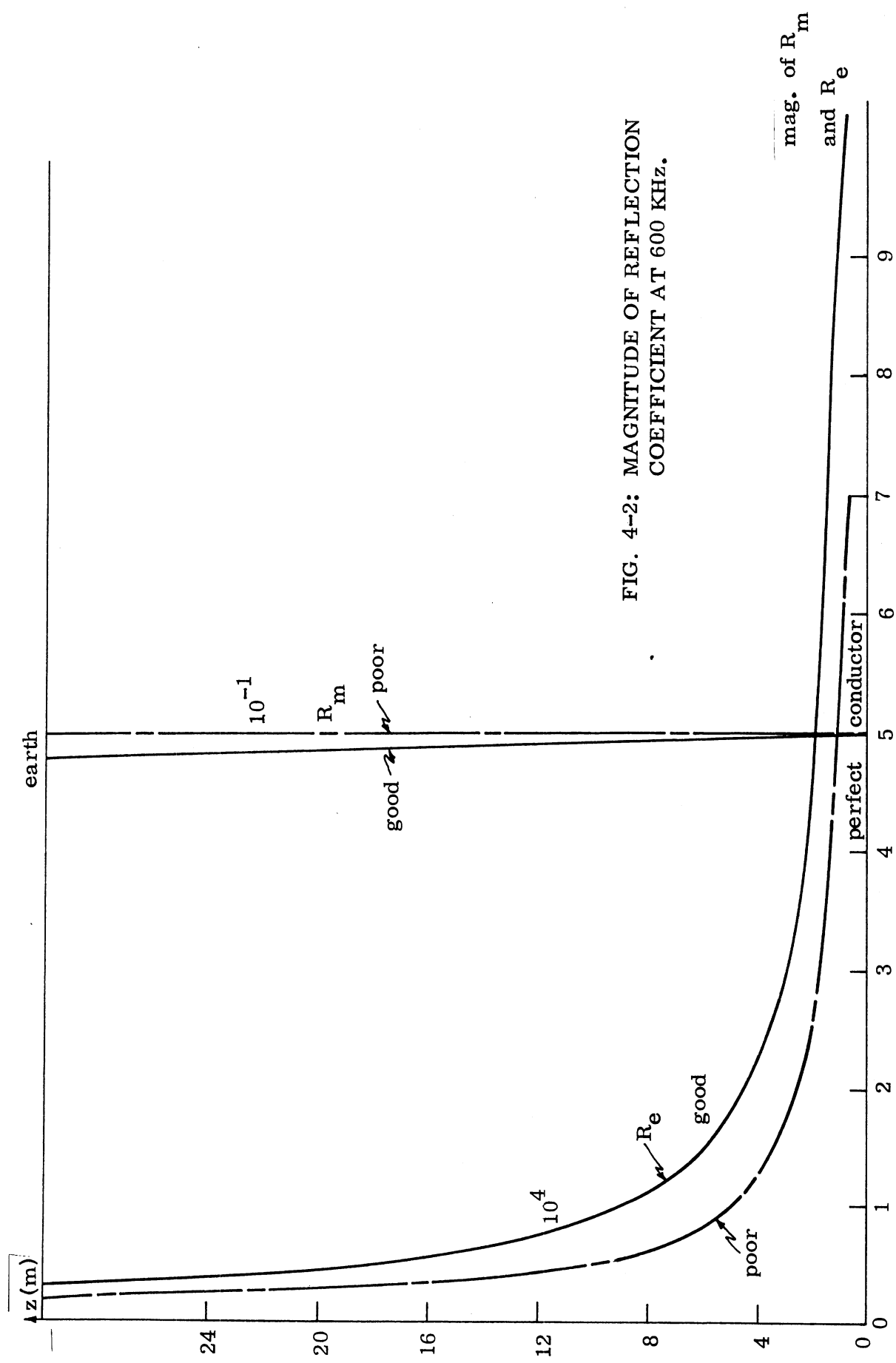
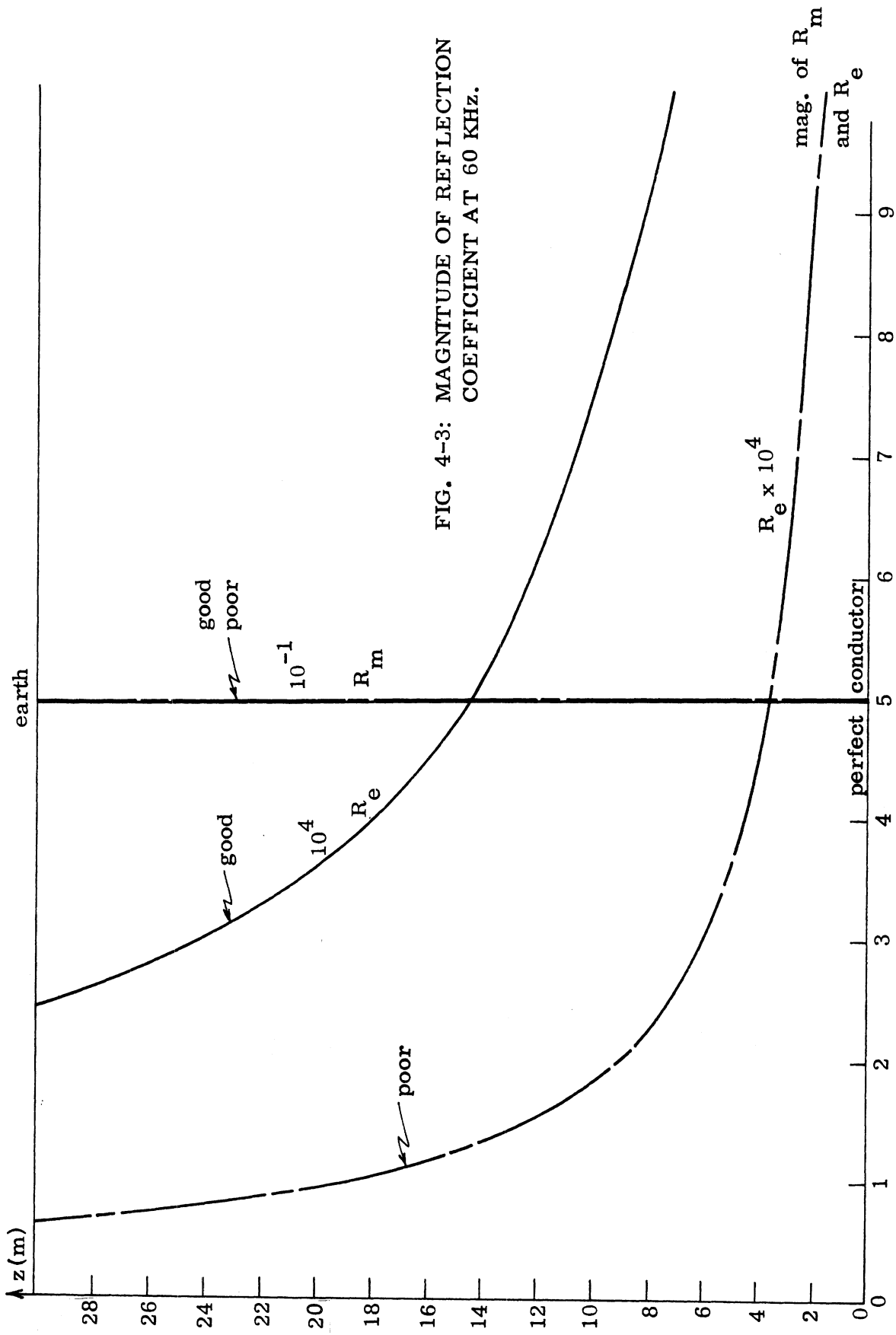


FIG. 4-2: MAGNITUDE OF REFLECTION COEFFICIENT AT 600 KHZ.



The percentage error for R_{eI} at $n^2 = 4 + i3$ is very large. The reason for this large value is the fact that the reflection coefficient R_e has a pole near this particular combination of n^2 and $\cos \theta$. While for the same combination the approximate function R_{eI} has the corresponding pole not as close as the exact one. Thus, for all points of observation near the poles of R_e , the error of using the impedance condition is large. Other than those particular points in general for $|n^2| > 5$, the error is less than 1 percent. For very large values of n the difference is negligible. The far-zone field is directly proportional to these coefficients so that the error in the far field in using R_{mI} and R_{eI} is of the same order of magnitude. They will be shown in the next section.

4.3 Far-Zone Field

The far-zone electric fields due to the vertical and horizontal electric dipoles are presented in this section. There are the E_r and E_z components corresponding to the vertical dipole and only the E_ϕ component corresponding to the horizontal dipole. They are shown in the same figure (with only $\phi = 90^\circ$ shown for the horizontal dipole case). Due to the use of the saddle point method, the fields obtained are in the far-zone. The definition of the far field in our research is $r \geq 15\lambda$. Thus, the range of the far-zone varies with the frequency. Hence the magnitudes of the fields are not in the same order of magnitude for three frequencies.

All curves of E_r , E_z and E_ϕ tilted forward near the dielectric surface compared to that at the conducting plate. Figures 4-4 and 4-7 show that E_ϕ is stronger for the poor earth than for the good earth. As the frequency is lowered the difference in E_ϕ with good earth and poor earth increases greatly. But the differences in E_z and E_r get smaller. This is directly related to the properties of R_m and R_e as discussed before. Figures 4-5, 4-6 clearly show that the curves of E_z and E_ϕ are almost perpendicular to both plates. In these two cases, the index of refraction of the earth is so large that it appears to be a perfect conductor.

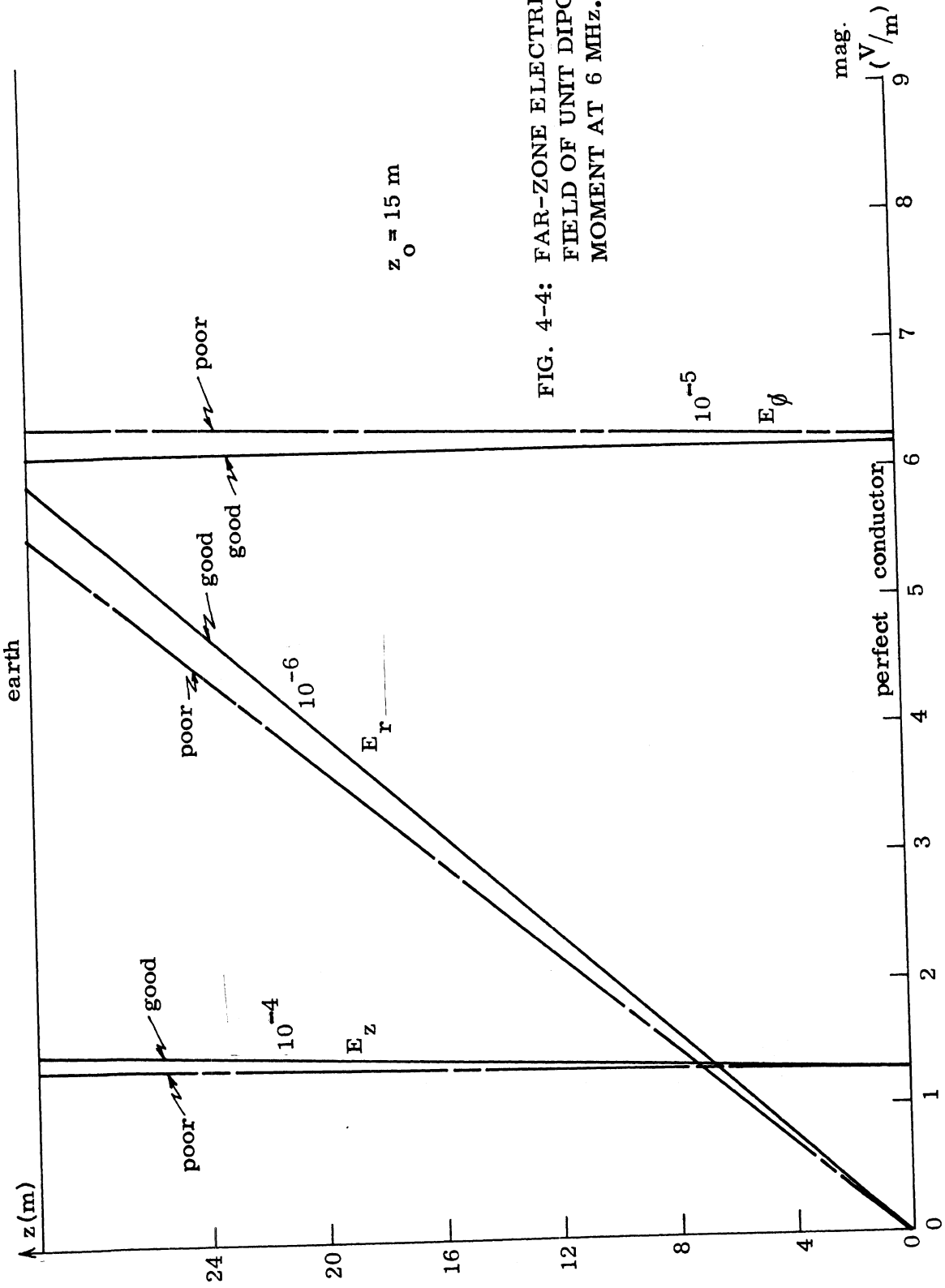


FIG. 4-4: FAR-ZONE ELECTRIC FIELD OF UNIT DIPOLE MOMENT AT 6 MHZ.

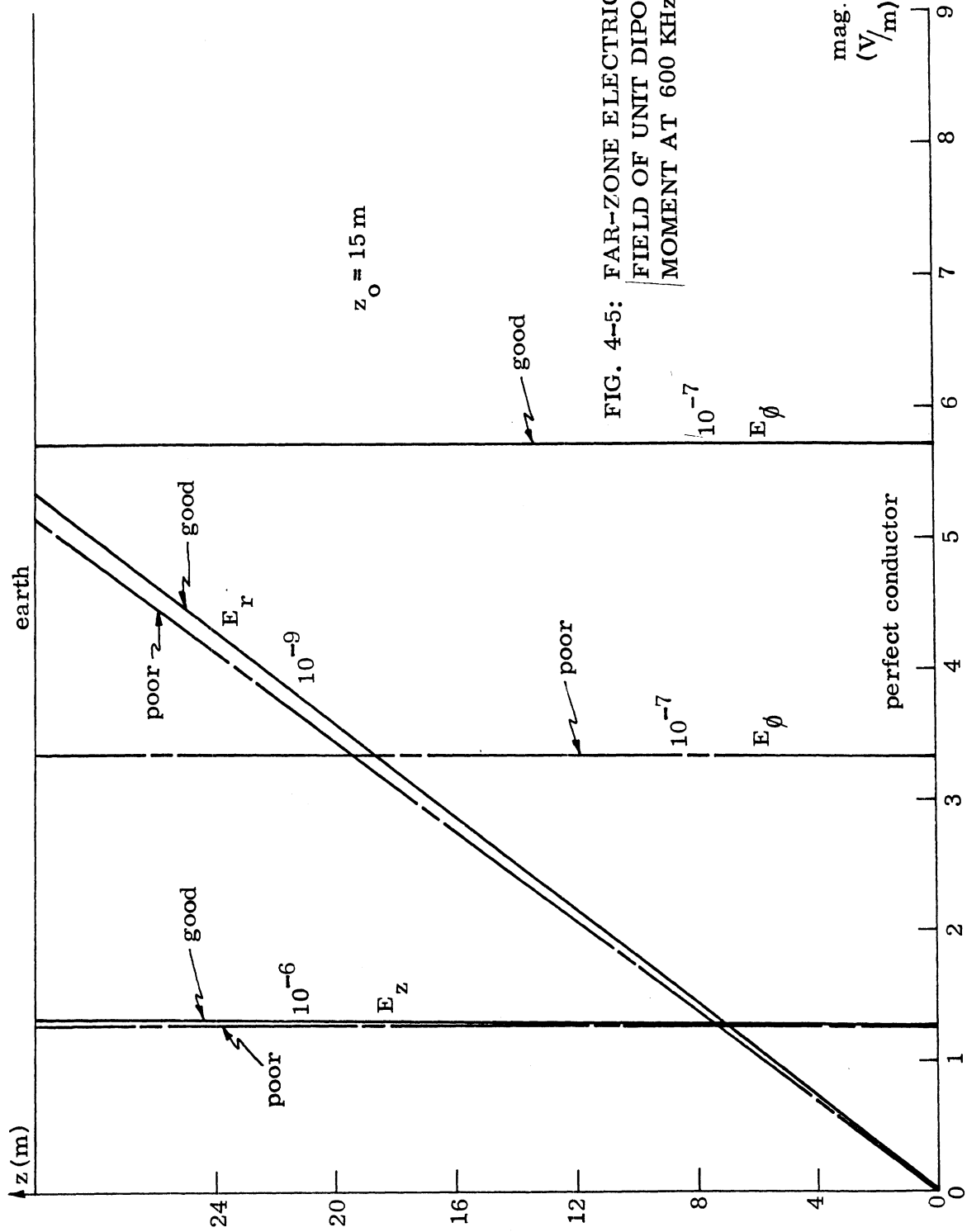
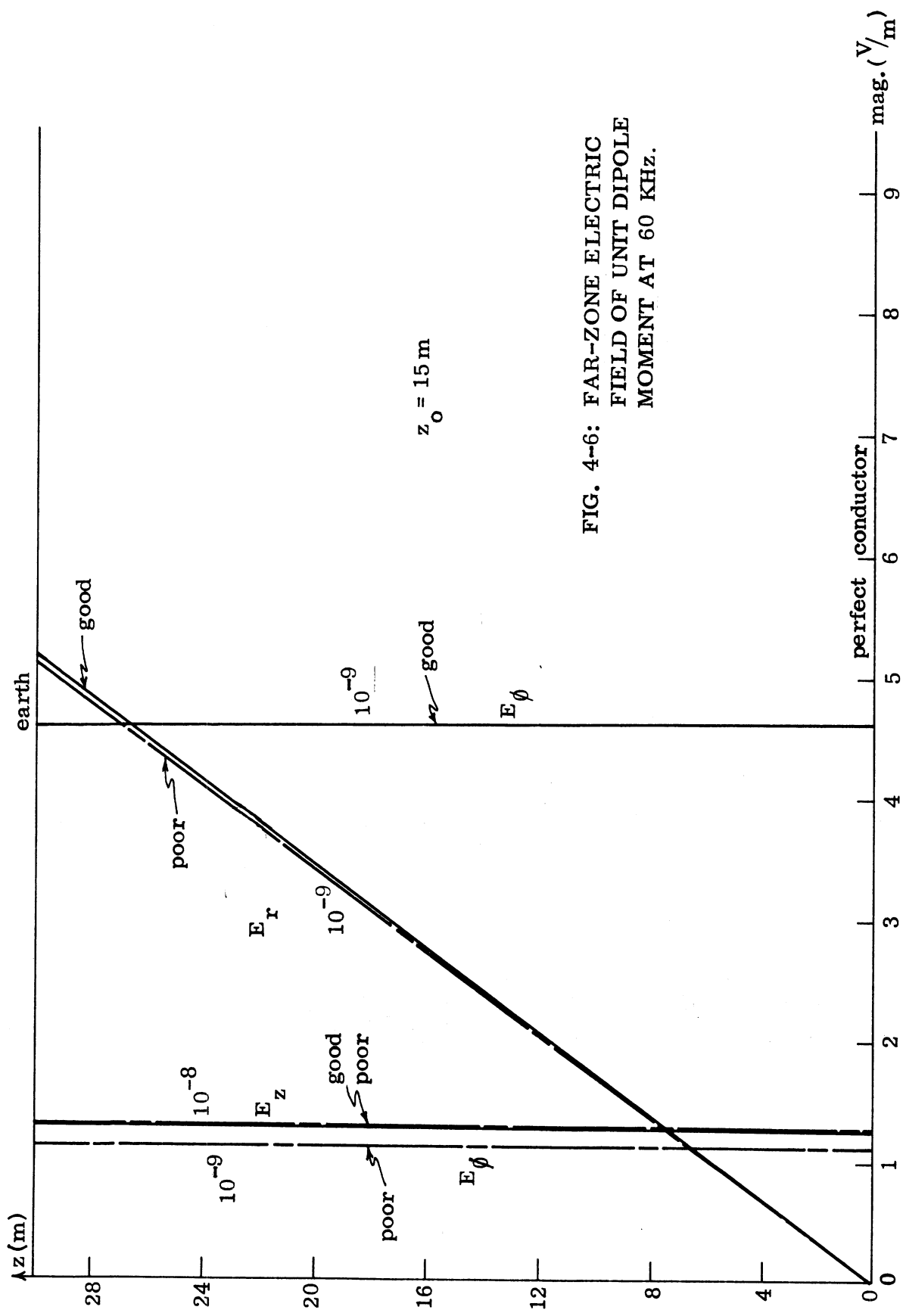


FIG. 4-5: FAB-ZONE ELECTRIC FIELD OF UNIT DIPOLE MOMENT AT 600 KHZ.



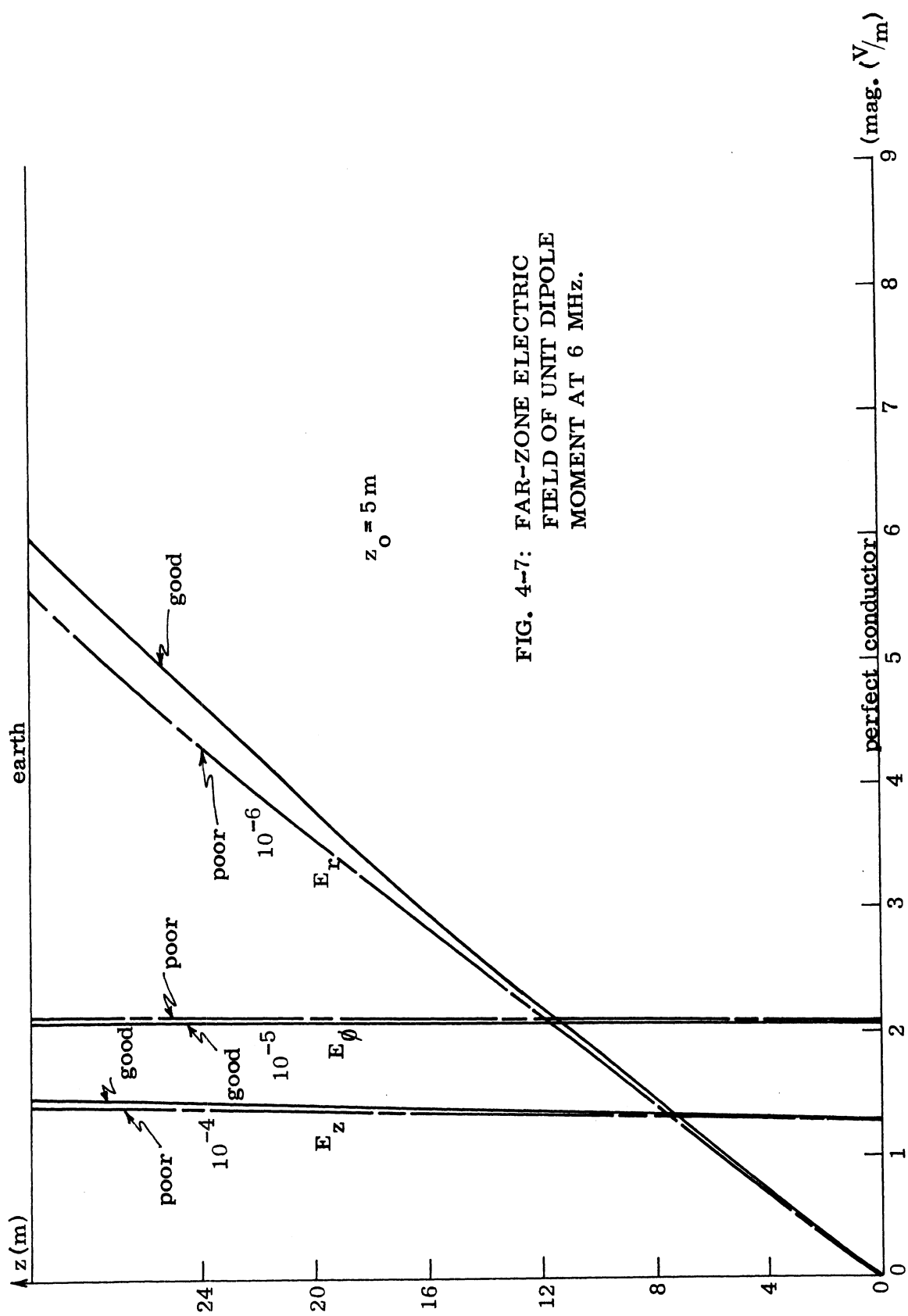


FIG. 4-7: FAR-ZONE ELECTRIC FIELD OF UNIT DIPOLE MOMENT AT 6 MHz.

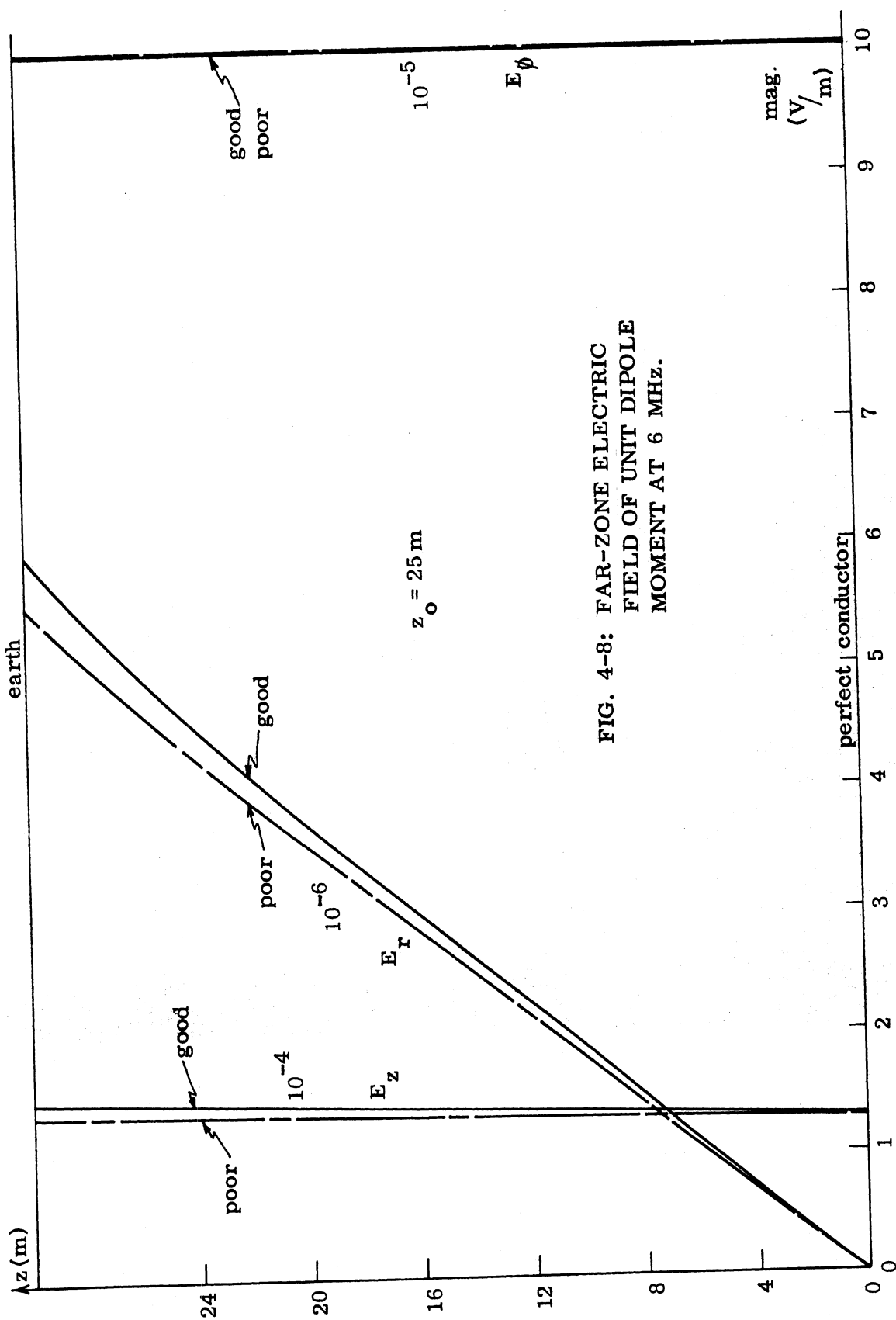


FIG. 4-8: FAR-ZONE ELECTRIC
FIELD OF UNIT DIPOLE
MOMENT AT 6 MHZ.

In Fig. 4-7, the dipole source is located near the perfect conductor at $z_0 = 5\text{m}$, all three electric field curves tilted forward more than in the case of a symmetrically located source. Figure 4-8 shows the results when the source is located near the dielectric surface. A much stronger E_ϕ is found. Since the separation distance L between the two plates is very small, there is no drastic change in the far field patterns as shown in the figures for different source locations.

The percentage error in the far field when using the impedance boundary condition is given below.

f	n^2	$\cos \theta$	% error of E_r	% error of E_z	% error of E_ϕ
6 MHz	$4+i0.3$	0.039	1.140	1.122	0.232
6 MHz	$10+i30$	0.039	0.240	0.221	0.065
600 KHz	$4+i3$	0.004	0.091	0.093	7.417
600 KHz	$10+i300$	0.004	0.0037	0.0027	0.0157
60 KHz	$4+i30$	0.0004	0.0019	0.0078	0.357
60 KHz	$10+i3000$	0.0004	0.0	0.0	0.0043

Table 4-3: Percentage Error for Far Field

4.4 Excitation Factor for Various Sources

Several difficulties have to be treated carefully when the problem involves lossy media. They are: how many components of the Hertz vectors are responsible for the field and what is the excitation factor for a given source. The advantages of using the dyadic Green's function technique is that it systematically solves electromagnetic problems in such a way that these questions are easily answered.

The dyadic Green's functions are chosen so that when applying the vector Green's theorem to the region concerned, the surface integral equals zero as a result of the boundary conditions and/or the radiation condition. Thus, the two field equations are

$$\bar{E} = i\omega\mu \iiint \bar{\bar{G}}_3(\bar{R}/\bar{R}') \cdot \bar{J}(\bar{R}') dV' ,$$

$$\bar{H} = k^2 \iiint \bar{\bar{G}}_4(\bar{R}/\bar{R}') \cdot \bar{m}(\bar{R}') dV' .$$

The dot product in the integrand shows explicitly which Hertz vector is involved and what is the excitation factor. For example, in Eq. (3.3), it is clear that for a z-directed electric dipole, only the $\bar{N}_{e0\lambda}$ function is needed to specify the field. This is in agreement with Sommerfeld's result; however, he used physical considerations to find this particular vector function. For an x-directed electric dipole, it is seen from Eq. (3.13) that the $\bar{N}_{o1\lambda}$ and $\bar{M}_{e1\lambda}$ functions, both of higher order, are necessary. This again agrees with Sommerfeld's discussion on the choice of the Hertz vectors for a horizontal dipole. For a detailed discussion, see Chapter 8 of reference [6].

As discussed above, the excitation factor for a given source is built into the Green's function. Since the radiated wave is composed of several different component waves, the excitation factor has several components. These components are directly related to the results of the integration as derived before. The excitation factors of the electric field for different kinds of sources are shown in Table 4-4. The pole location, $R + i\theta_i$, is discussed in the next section. For completeness, the propagation factor of the surface wave is derived in Eq. (A-1).

Thus, both difficulties are solved at the same time. These features, which avoid all the determination works on how to choose the potential functions and the excitation factors, show that the dyadic Green's function technique is more systematic.

source type	direct and reflected wave	surface wave (mode factor)
z-directed electric dipole	$\frac{\omega \mu_0 I \ell}{4\pi} \sin \theta \cos(kz_o \cos \theta) \hat{\theta}$	$-\text{i} \omega \mu_0 I \ell k^{1/2} \sin^3/2(\theta_R + i\theta_i) \cos [kz_o \cos(\theta_R + i\theta_i)] x \\ x \sqrt{-2i} \hat{\theta}$
x-directed electric dipole	$\frac{\omega \mu_0 I \ell}{4\pi} \sin(kz_o \cos \theta) x \\ x \left\{ \sin \phi + \cos \theta \cos \phi \hat{\theta} \right\}$	$i \omega \mu_0 I \ell k^{1/2} \sin^3/2(\theta_R + i\theta_i) \sin [kz_o \cos(\theta_R + i\theta_i)] x \\ x \sqrt{-2i} \left\{ \sin \phi \hat{\phi} + \cos(\theta_R + i\theta_i) \cos \phi \hat{\theta} \right\}$
horizontal current loop	$\frac{IAk^2}{4\pi} \sin \theta \sin(kz_o \cos \theta) \hat{\theta}$	$iIAk^{5/2} \sin^3/2(\theta_R + i\theta_i) \cos [kz_o \cos(\theta_R + i\theta_i)] x \\ x \sqrt{-2i} \hat{\theta}$
vertical current loop	$-\frac{IAk^2}{4\pi} \cos(kz_o \cos \theta) x \\ x \left\{ \sin \hat{\phi} + \cos \theta \cos \phi \hat{\theta} \right\}$	$-iIAk^{5/2} \sin^3/2(\theta_R + i\theta_i) \sin [kz_o \cos(\theta_R + i\theta_i)] x \\ x \sqrt{-2i} \left\{ \sin \phi \hat{\phi} + \cos(\theta_R + i\theta_i) \cos \phi \hat{\theta} \right\}$

Table 4-4: TABLE OF EXCITATION FACTOR FOR WAVE COMPONENTS
FOR DIFFERENT SOURCES.

4.5 Distribution of Poles in the Complex θ Domain

When considering wave propagation, it is necessary to discuss the properties of mode poles. For guides with perfectly conducting walls, the poles are either on the real axis of the complex θ domain, corresponding to propagating modes, or on the imaginary axis, corresponding to evanescent modes. These poles can be found from the fundamental equation of mode theory. For example, the equation satisfied by TM waves is

$$kL \cos \theta = \pm m\pi \quad \text{where } m = \text{integer.}$$

When one plate of the waveguide is not perfectly conducting, the mode equation is represented by Eq. (3.9)

$$\frac{h_E}{n^2 h} = i \tan(hL) .$$

By using Newton Raphson's method (Appendix B), the solutions for the propagation constants of quasi-evanescent modes can be obtained. The impedance boundary condition is used to get an approximate solution for the modes in Eq. (3.10) which yields

$$\frac{h}{nk} = i \tan(hL) .$$

The locations of these poles are also obtained here. They are shown in the following table for comparison. In general, for the same operating frequency, the higher the value of the refractive index n the closer the approximate solution is to the exact solution. This points out again the necessary assumption for the proper application of the impedance boundary condition. In the case of the poor earth at 60 KHz ($n^2 = 10 + i3000$), due to the large value of n , it is logical to assume that the poles will be located very close to those of the perfectly conducting case. However, the imaginary part of the pole is very large compared to zero as shown in Table 4-4. Notice that particular frequency is very far from the cut-off frequency, 5 MHz in our study. Thus, the electric length between the guides plays an important role as well as the refractive index n .

frequency	mode number	complex θ ($\theta_R + i\theta_i$)		
		perfect conductor	exact	approximate
6 MHz $(n^2 = 10 + i30)$	0	$1.5708 + i0$	$1.447 + i0.1930$	$1.448 + i0.1949$
	1	$0.585 + i0$	$0.6457 + i0.08229$	$0.6463 + i0.0822$
	2	$0 + i1.094$	$0.0176 + i1.086$	$0.0178 + i1.086$
600 KHz $(n^2 = 10 + i300)$	0	$1.5708 + i0$	$1.425 + i0.3568$	$1.426 + i0.3569$
	1	$0 + i2.81$	$0.00144 + i2.808$	$0.0016 + i2.808$
60 KHz $(n^2 = 10 + i3000)$	0	$1.5708 + i0$	$1.346 + i0.619$	$1.346 + i0.619$

Table 4-4: Location of Poles for Good Earth ($\sigma = 10^{-2} \text{ S/m}$)

frequency	mode number	complex θ ($\theta_R + i\theta_i$)		
		perfect conductor	exact	approximate
6 MHz $(n^2 = 4 + i0.3)$	0	$1.5708 + i0$	$1.289 + i0.1713$	$1.267 + i0.169$
	1	$0.585 + i0$	$0.6021 + i0.2817$	$0.5913 + i0.2927$
	2	$0 + i1.094$	$0.0745 + i1.101$	$0.0611 + i1.102$
600 KHz $(n^2 = 4 + i3)$	0	$1.5708 + i0$	$1.106 + i0.8015$	$1.078 + i0.8752$
	1	$0 + i2.81$	$0.0575 + i2.775$	$0.0166 + i2.805$
60 KHz $(n^2 = 4 + i30)$	0	$1.5708 + i0$	$1.153 + i1.481$	$1.180 + i1.514$

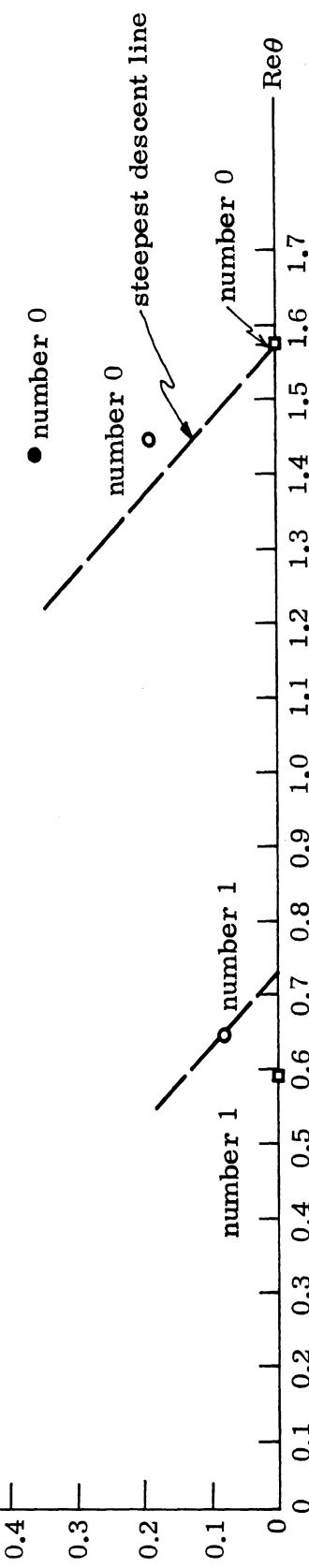
Table 4-5: Location of Poles for Poor Earth ($\sigma = 10^{-4} \text{ S/m}$)

Since the path of integration in the complex θ plane is deformed when evaluating the integral, it is convenient to plot the pole distribution in the same plane for the discussion of surface waves. The pole locations for our problem are shown in Figs. 4-9 and 4-10.

Note that the number 1 pole for the good earth case in Fig. 4-9 has a much smaller imaginary part than that of the number 0 pole. The opposite is true for the poor earth case as shown in Fig. 4-10. The steepest descent line



FIG. 4-9: POLE DISTRIBUTION FOR GOOD EARTH.



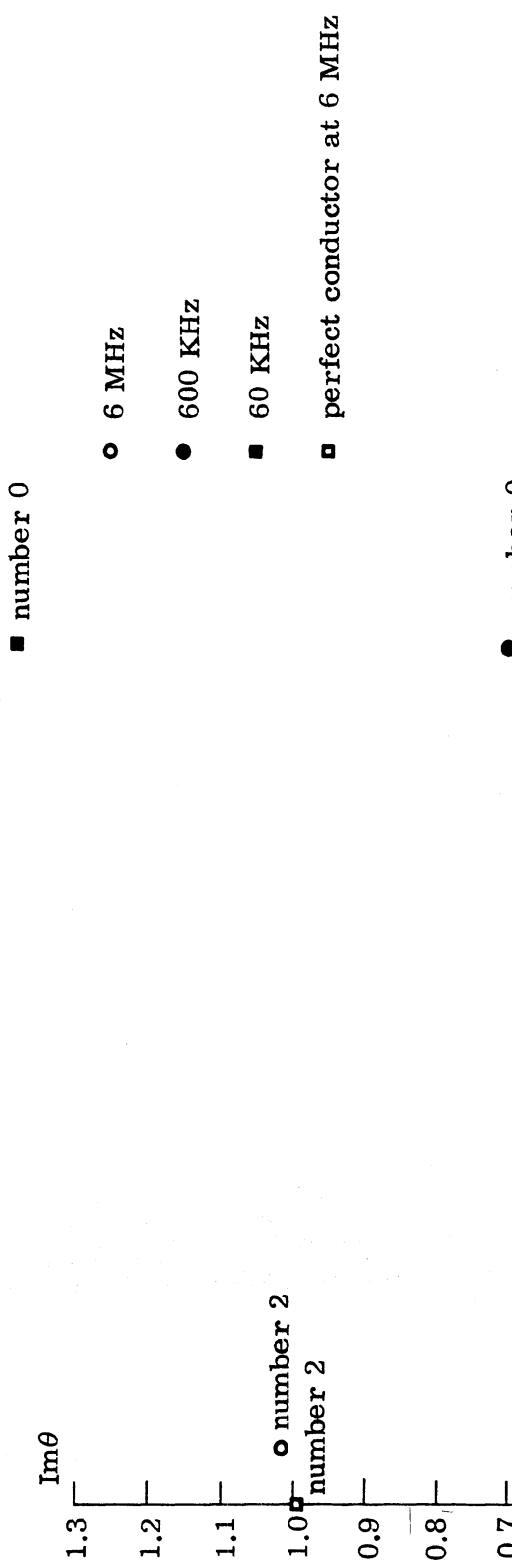
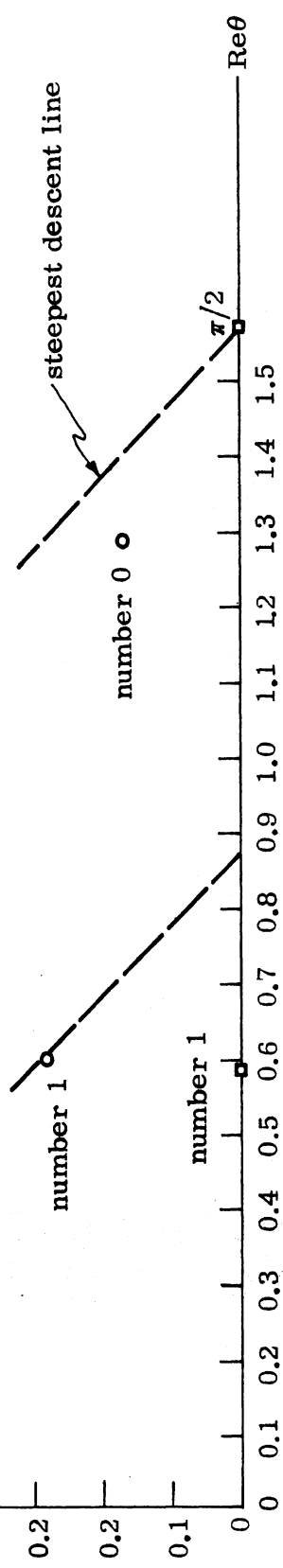


FIG. 4-10: POLE DISTRIBUTION FOR POOR EARTH.



has an inclination of 45° with the real axis for any point of observation. Thus, when the observation point is beyond $\theta = 41.8$, for the good earth case, the contribution of the number 1 pole has to be taken into account. However, since the number 0 pole is on the right hand side of the steepest descent line, this pole contributes nothing to the field for any observation angle. Thus, the strength of the surface wave depends only on the imaginary part of pole number one. The dependence of the surface wave upon the location of the pole is discussed in Appendix C.

In the case of poor earth, both poles, number 0 and number 1, enter into the picture when the observation angle is larger than 49.8° and less than 90° . Because the imaginary part of the number 0 pole is much smaller than that of number 1, it is evident that the number 0 mode is the dominant one. However, if the observation angle is greater than 49.8° and less than 83.6° , only mode number 1 contributes, so it is the dominant mode. Thus one has to be careful in discussing wave propagation when lossy media are involved. The zeroth order mode does not always supply the dominant contribution to the surface wave as suggested by some authors. It is possible that during the deformation of the integration path no pole is swept through until θ has a certain value. Then it is clearly seen that no significant surface waves exist when the observation point is less than certain angle. For example, for $\theta \lesssim 41^\circ$ in our two cases, only the direct and the reflected waves exist even in the near zone.

CHAPTER V

CONCLUSIONS AND RECOMMENDATIONS

5.1 Conclusions

In this thesis we have developed the technique of using the dyadic Green's function method to solve a particular problem in wave propagation. We have found the exact integral form of the fields due to various simple Hertzian dipoles in between two parallel plates with different material and the asymptotic solution associated with them.

The use of the Leontovich impedance boundary condition at the lossy interface is discussed. The percentage error in using this condition compared to the use of the exact boundary condition is calculated. Except when the point of observation is near a mode pole, the higher the refractive index the lower the percentage of error.

The pole contribution of the Green's function technique is shown to be the same as the mode contribution of the waveguide theory. A detailed study on the pole distribution in complex θ domain leads to the conclusion that it is premature to predict which mode is dominant before actually examining the pole location.

The symmetry property of the dyadic Green's function in a two layer problem is proved. The same procedure could easily be extended to other many-body systems.

5.2 Areas for Future Study

In the present investigation the exact integral formulation of a parallel plate waveguide problem is derived. The far-zone field is calculated by the saddle point method, which is only the asymptotic expression. When the time domain solution is needed, the high frequency, intermediate frequency and the low frequency solutions are required for the application of Fourier transform. Thus, the exact integration for all frequencies needs to be derived. The technique of performing this infinite integral is an interesting problem and worth further investigation.

Another area for future work would be the efficiency problem. According to the study in section 4.3., the far-zone field is slightly affected by the source location z_0 . However, the portion of energy entering into the lossy dielectric is directly related to the source location. It is very useful for the simulation test designer to understand the distribution of power and the efficiency of a simulator [21].

REFERENCES

- [1] Watson, G. N. (1919), "The transmission of electric waves round the earth," Proc. Roy. Soc., 95, p. 546.
- [2] Bremmer, H. (1949), Terrestrial Radio Waves, Elsevier, Amsterdam, Netherlands.
- [3] Budden, K. G. (1961), The Wave-Guide Mode Theory of Wave Propagation, Prentice Hall, Englewood Cliffs, N. J.
- [4] Budden, K. G. (1962), Radio Waves in the Ionosphere, Cambridge University Press, London.
- [5] Wait, J. R. (1962), Electromagnetic Waves in Stratified Media, Permagon Press, New York.
- [6] Tai, Chen-To (1971), Dyadic Green's Functions in Electromagnetic Theory, International Textbook Company, Scranton, Penna.
- [7] Tai, Chen-To (1973), "On the eigenfunction expansion of dyadic Green's functions," IEEE Proceedings, No. 4, p. 480.
- [8] Schwinger, J. (1943), "Fourier transform solution of integral equations," M.I.T. Radiation Laboratory Report 43, 44.
- [9] Levine, H. and J. Schwinger (1950), "On the theory of electromagnetic wave diffraction by an aperture in an infinite plane conducting screen," Comm. Pure and Appl. Math., III, No. 4, p. 355.
- [10] Morse P. M. and H. Feshbach (1953), Methods of Theoretical Physics II, McGraw-Hill, New York, chap. 13.
- [11] Tai, Chen-To (1954), "A glossary of dyadic Green's functions," Stanford Research Institute Technical Report No. 46.
- [12] Fock, V. (1946), "The field of a plane wave near the surface of a conducting body," Jour. of Phys., Vol. X, 5, p. 399.
- [13] Leontovich, M. A. (1948), Investigations of Propagation of Radiowaves, Moscow.
- [14] Feynberg, Ye. L. (1961), The Propagation of Radio Waves Along the Surface of the Earth, Clearinghouse Translation 1967.
- [15] Hiatt, R. E., T. B. A. Senior and V. H. Weston (1960), "Studies in radar cross sections XL-surface roughness and impedance boundary conditions," The University of Michigan Radiation Laboratory Report 2500-2-T.
- [16] Sommerfeld, A. (1949), Partial Differential Equations, Academic Press, New York, p. 197.

- [17] Felsen, L. B. and N. Marcuvitz (1973), Radiation and Scattering of Waves, Prentice Hall, Englewood Cliffs, N. J., p. 465.
- [18] Nomura, Y. (1953), "On the theory of propagation of electric waves over a plane surface of the homogeneous earth," Reports of the Research Institute of Electrical Communication, Tohoku University, Japan, Vol. 5, No. 3, 4, p. 203.
- [19] Van der Waerden, B. L. (1951), "On the method of saddle points," Applied Sci. Res., B2, p. 33.
- [20] Stratton, J. A. (1941), Electromagnetic Theory, McGraw-Hill, New York, p. 235.
- [21] Hansen, P. M. (1970), "The Radiation Efficiency of a Dipole Antenna Above an Imperfectly Conducting Earth," Ph.D. Thesis, University of Michigan.
- [22] Carnahan, B., H. A. Luther and J. O. Wilkes (1969), Applied Numerical Methods, John Wiley and Sons, New York, p. 319.

APPENDIX A
GENERAL DISCUSSION ON SADDLE POINT INTEGRATION

In Chapter III, we discussed the situation where the path of steepest descent does not cross over a singularity. In general, when we deform the integration path to that of the steepest descent, it sweeps through some poles and branch cuts. In this appendix, we discuss the general characteristics of the field distribution due to these two kinds of singularities. It is found that the contribution to the field of these singularities under our assumptions is negligible provided that kr is greater than 20π .

Since the saddle point integration always involves multi-valued functions it is worthwhile to consider several often neglected points about branch cut integrals and contour integration. We follow closely the method discussed in reference 17.

The reason we chose the branch cut along the lines of $\operatorname{Re} \sqrt{k^2 - \lambda^2} = 0$ and $\operatorname{Re} \sqrt{n^2 k^2 - \lambda^2} = 0$ in section 3.2.1 was that we could have unique analytic property in each quadrant of the complex λ plane. The analytic property of $\sqrt{k^2 - \lambda^2}$ on the uppermost Riemann sheet in the complex λ domain is

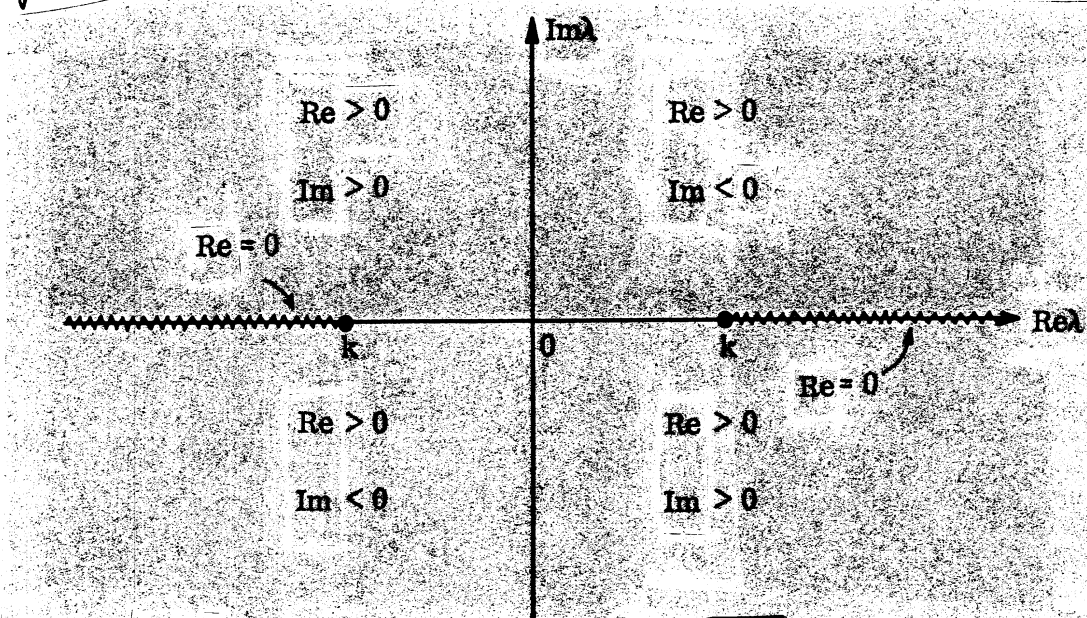


FIG. A-1: BRANCH CUT ALONG $\operatorname{Re} \sqrt{k^2 - \lambda^2} = 0$.

Recall that the integral converges only when the imaginary part is greater than zero. Thus, it is clear that the path of integration must pass through the second and fourth quadrants only. There is no way that we can close the contour along a semi-infinite circle; hence the Cauchy residue theorem can never be applied.

In the discussion of multi-valued functions, in general, the roots of one equation have to be checked to assure that some roots are indeed the poles of that equation. The advantage of this kind of choice of the branch cut is to insure that the roots of the reflections coefficient equation are indeed the poles on this particular Riemann sheet [18]. An alternative way of choosing the branch cut is along the line of $\text{Im} \sqrt{k^2 - \lambda^2} = 0$. The analytic properties of $\sqrt{k^2 - \lambda^2}$ in the complex λ domain are shown in Fig. A-2.

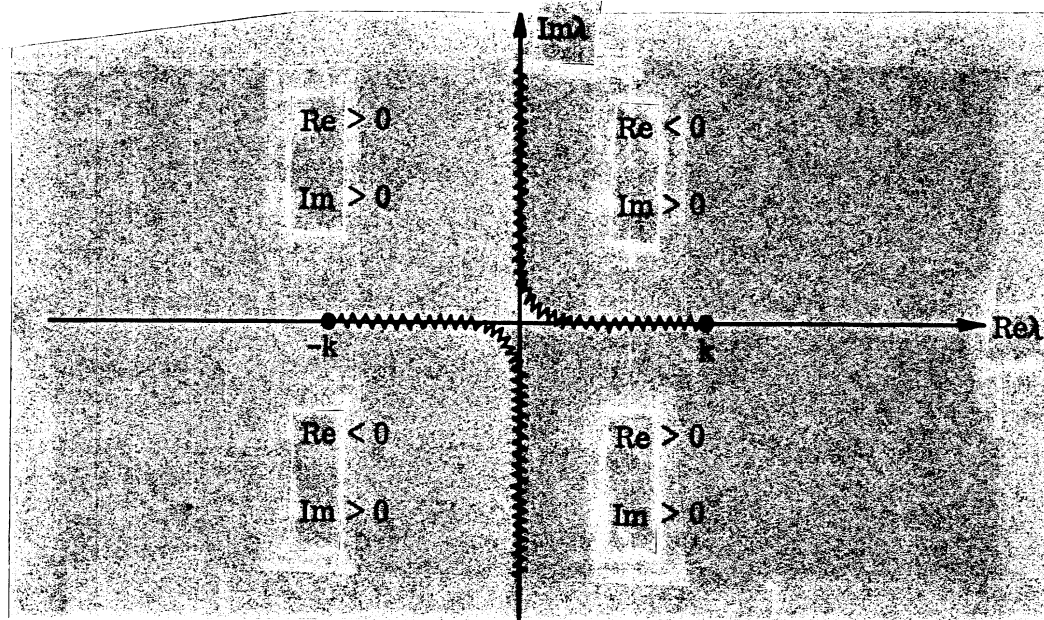


FIG. A-2: BRANCH CUT ALONG $\text{Im} \sqrt{k^2 - \lambda^2} = 0$.

Again, each quadrant has the unique property in its whole quadrant range. Since the imaginary part of the function is greater than zero everywhere on this Riemann sheet, the integration path could be everywhere in that sheet. Hence the contour can be closed and the Cauchy residue theorem so applied. In

general, the roots of the equation will be the poles of that equation on this Riemann sheet 18 .

In some of the literature, the choice of the branch cut is parallel to the imaginary axis. This choice is neither along the real part being zero nor along the imaginary part being zero. The analytic properties in the complex λ plane are shown in Fig. A-3.

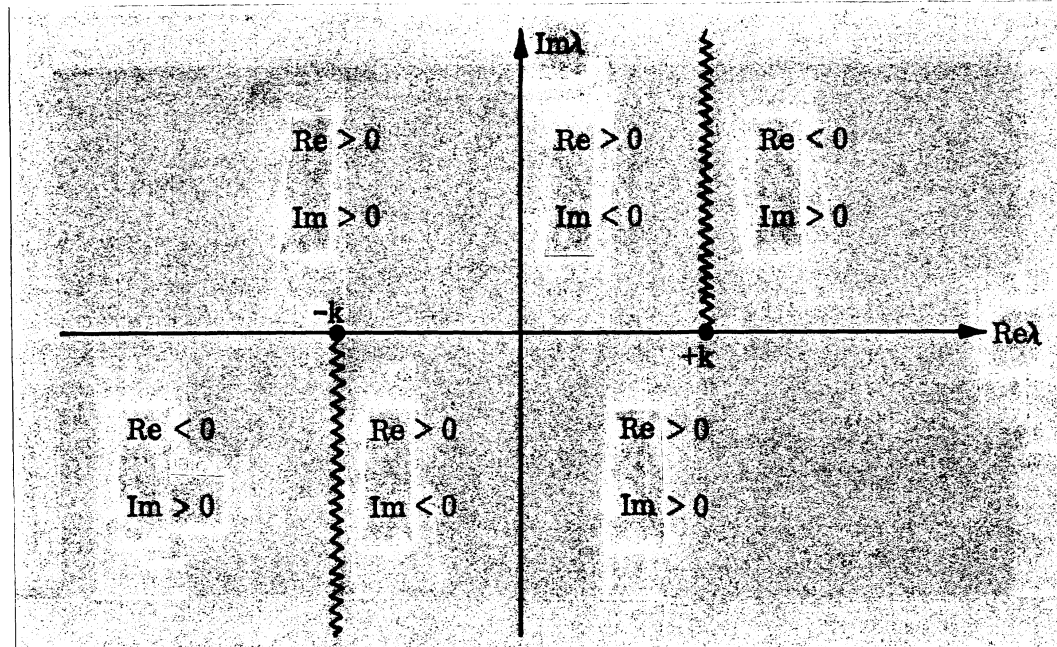


FIG. A-3: BRANCH CUT PARALLEL TO IMAGINARY AXIS.

There are two regions corresponding to the first and the third quadrant which exhibit different analytic properties. Thus, again the closure of the contour can not be used. Similarly, the transformation $\lambda = k \sin \beta$ maps this mixed property into the complex β plane. Hence, special attention has to be given to the region of convergence of the integral. Thus, there is no advantage at all for this particular choice.

We recall in Section 3.2.1 that when the path of integration is deformed from C to C_S in the complex β domain, it is possible to cross some singularities. In this case, the path is plotted as follows:

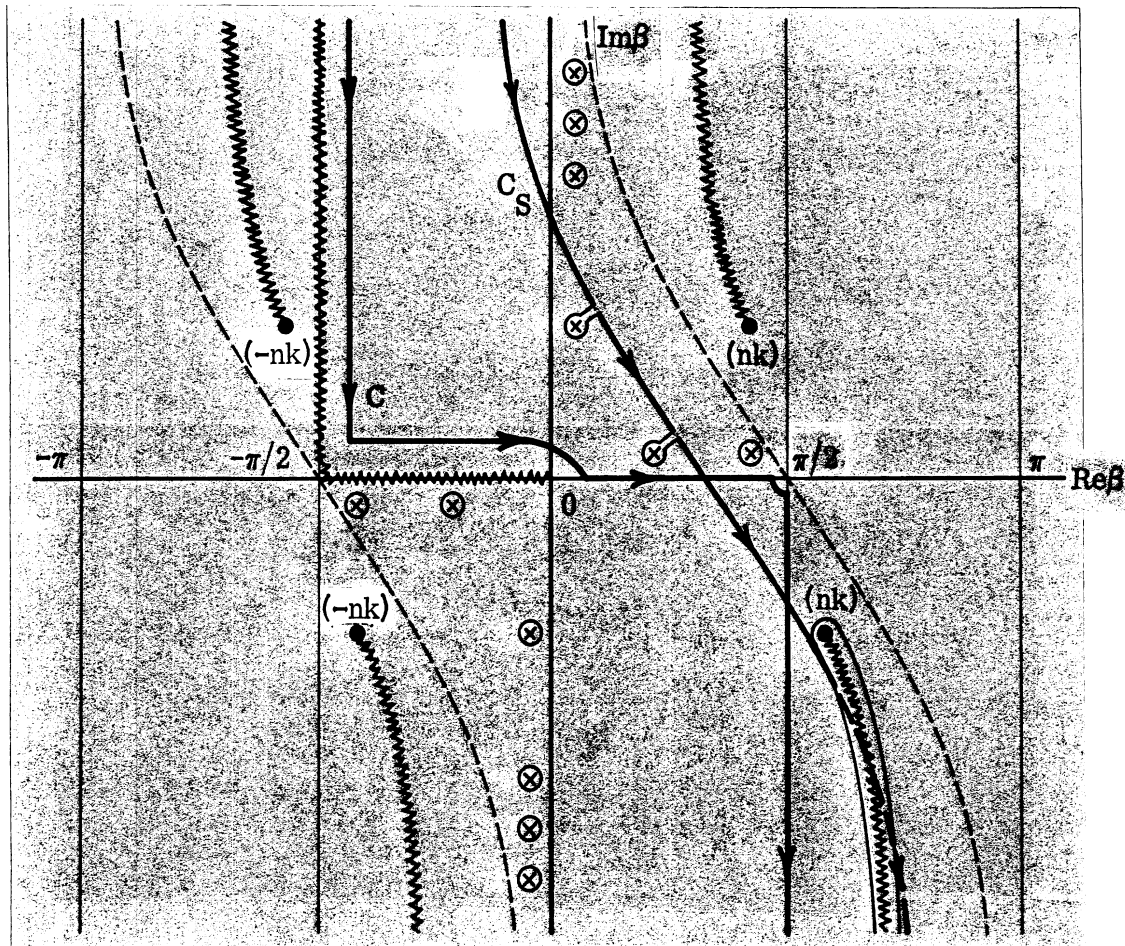


FIG. A-4: INTEGRATION PATH IN COMPLEX β PLANE.

Rewriting the integration in the complex β domain for the case of a vertical electric dipole:

$$\bar{E} \approx -\frac{\omega \mu_0 I l}{4\pi k} \int_{-\frac{\pi}{2}+i\infty}^{\frac{\pi}{2}-i\infty} d\beta \frac{3}{k^2} \sin^3 \beta 2 \cos(kz_0 \cos \beta) \sqrt{\frac{-2i}{\pi R \sin \theta}} \left\{ 1 + S \left| \begin{array}{l} k \cos \beta \\ -k \cos \beta \end{array} \right| \right\} e^{ikR \cos(\theta-\beta)} (\hat{z} \sin \beta - \hat{r} \cos \beta)$$

where

$$S = \frac{(h \frac{k^2}{E} - k^2 h_E) e^{ihL}}{2 \left[k^2 h_E^2 \cos(hL) - i k_E^2 h \sin(hL) \right]} .$$

$$\text{Res} \left[S \Big|_{k \cos \beta} - S \Big|_{-k \cos \beta} \right] = \frac{n^2 \cos \beta \cos(kL \cos \beta) - i\sqrt{n^2 - \sin^2 \beta} \sin(kL \cos \beta)}{\sqrt{n^2 - \sin^2 \beta} \cos(kL \cos \beta) - i n^2 \cos \beta \sin(kL \cos \beta)}.$$

The roots of the coefficient equation which are the poles of this equation on this Riemann sheet could be found by using the Newton-Raphson's method [22]. The pole location of the problem concerned was shown in Figs. 4-9 and 4-10. The numerical value of the pole is represented by $\theta_R + i\theta_i$. Thus, the contribution to the residue by the coefficient equation is:

$$\text{Res} \left[S \Big|_{k \cos \beta} - S \Big|_{-k \cos \beta} \right] = \frac{n^2 \cos \beta \cos(kL \cos \beta) - i\sqrt{n^2 - \sin^2 \beta} \sin(kL \cos \beta)}{\frac{d}{d\beta} \left[2(\sqrt{n^2 - \sin^2 \beta}) \cos(kL \cos \beta) - i n^2 \cos \beta \sin(kL \cos \beta) \right]} \Bigg|_{\beta = \theta_R + i\theta_i}$$

The field due to the contribution of the pole is:

$$\bar{E} \approx - \sum_p i \omega \mu_0 I \ell k^2 \sin^{\frac{1}{2}}(\theta_R + i\theta_i) \cos \left[kz_0 \cos(\theta_R + i\theta_i) \right] \sqrt{\frac{-2i}{\pi R \sin \theta}} \times \\ x \left\{ 1 + \text{Res} \left[S \Big|_{k \cos \beta} - S \Big|_{-k \cos \beta} \right] \right\} \left\{ \hat{z} \sin(\theta_R + i\theta_i) - \hat{r} \cos(\theta_R + i\theta_i) \right\} \\ \cdot e^{ikR \cos(\theta - \theta_R - i\theta_i)}.$$

From the exponential function:

$$ikR \cos(\theta - \theta_R - i\theta_i) = ikR \left[\left(\cos \theta \cos \theta_R + \sin \theta \sin \theta_R \right) \cosh \theta_i + \right. \\ \left. + i \left(\sin \theta \cos \theta_R - \cos \theta \sin \theta_R \right) \sinh \theta_i \right] \quad (\text{A.1})$$

we find that the decaying factor is given by:

$$\text{Exp} \left[-kR \sinh \theta_i \left(\sin \theta \cos \theta_R - \cos \theta \sin \theta_R \right) \right]. \quad (\text{A.2})$$

From the discussion in section 4.5, only one pole contributes significantly for the good earth case at 6 MHz. The other poles have a large imaginary

part corresponding to highly attenuated waves. To calculate the surface wave field due to the pole contribution, the values are read from Fig. 4-9 as $\theta = 85^\circ$, $\theta_R + i\theta_i = 0.64 + i0.08$. In the far-zone region, the minimum distance is 10λ away, which implies that $kR = 62.8$. Substituting these figures into (A.1) gives the decaying factor of the order $1/55$, which is less than two percent of the total field.

For the case of good earth at 600 KHz, the number 0 pole is never crossed during the deformation of the path of integration. Only those poles with large imaginary part are crossed, which implies that these waves never travel too far.

As shown in Fig. A-4, the deformed path of integration could sweep through a branch cut. It simply means that the path of integration has to travel along the cut to infinity and cross the cut onto the second Riemann sheet. Since this branch cut corresponds to the singularity at nk , which does not occur in the exponential term of the integrand. This function has identical decay characteristics on either Riemann sheet. The contribution due to the branch cut depends greatly on the value of n and kr . According to Felsen [17], the contribution behaves in the order of $(kR)^{-3/2}$. For the problem with which are concerned, it is of the order $1/490$ in the far-zone. That means that the lateral wave field due to the branch cut is smaller than the surface wave field; hence, it too can be neglected.

The previous discussion holds only for the far-zone field. If the near-zone field is considered, then some poles may contribute significantly to the field. The same applies to the contribution by the branch cut.

When a pole singularity is near the saddle point of the integrand, the modified saddle point integration method has to be adopted. For detailed information, see reference [17] and [19].

APPENDIX B

NEWTON-RAPHSON'S METHOD

Newton-Raphson's method, an iterative method of solving nonlinear equations, is used here to find the zeroes of a complex valued function.

To find the zeroes of the following equation

$$F(z) = 0 \quad \text{where } z = x + iy ,$$

we separate the equation into real and imaginary parts.

$$F(x, y) = f_1(x, y) + if_2(x, y) = 0$$

where f_1 and f_2 are real functions. Then we arbitrarily choose a pair of trial solutions x , y , and substitute them into f_1 and f_2 . After this iteration, a pair of increments Δx , Δy results, which is given by

$$\Delta x = \frac{f_2 \frac{\partial f_1}{\partial y} - f_1 \frac{\partial f_2}{\partial y}}{D}$$

$$\Delta y = \frac{f_1 \frac{\partial f_2}{\partial x} - f_2 \frac{\partial f_1}{\partial x}}{D}$$

where

$$D = \frac{\partial f_1}{\partial x} \frac{\partial f_2}{\partial y} - \frac{\partial f_1}{\partial y} \frac{\partial f_2}{\partial x} .$$

Then the next approximations are:

$$x_1 = x + \Delta x$$

$$y_1 = y + \Delta y .$$

Substituting these values into the original equations f_1 and f_2 , we can proceed in a similar fashion to determine the higher order approximation.

Under certain restrictions [22], both functions f_1 and f_2 will converge to a certain preassigned small value. Then, this is the pair of approximate solutions of the complex equation we wish to solve. The programming of this method to our problem in the FORTRAN language is given in Appendix D.

APPENDIX C

DISCUSSION OF POLE DISTRIBUTION

In mode theory, the value of θ for a given mode can be represented as a point in the complex θ plane. The real and imaginary components of θ determine the phase velocity and the attenuation rate of the surface wave as shown in Appendix A. More importantly, the location of the pole can be used to determine whether it would be swept through during the deformation of the integration path. When a pole is swept through, there arises a Heaviside function which equals unity, implying that the pole contribution should be taken into account. Thus, the location of the pole can lead us to the delimited regions where the pole contribution could be observed.

In this Appendix, we discuss the pole locus of the problem of wave propagation between two parallel plates, one of which is perfectly conducting. There are two loci of poles presented for the TM waves. For each case, the frequency and the separation distance are kept constant.

Figure C-1 shows the particular case at cut-off frequency corresponding to a guide formed by two perfectly conducting plates. The dotted line represents the case when one plate represents the surface of a pure dielectric media whose refractive index has zero imaginary component. The broken line represents the case where the real part of the refractive index is very close to unity which corresponds to free space. The direction of the arrow indicates that the imaginary part of the refractive index is decreasing. In the limit both curves end up at $n^2 = 1 + i0$, which is the free space case. This case implies the absence of the second plate, hence, an open region. Thus, there is no mode occurring when a wave propagates above an infinite perfectly conducting plate.

It is clearly seen that the locus of the pole, when the other boundary represents an arbitrary kind of material, has to be inside the range defined by the above two limits. For number 0 mode, there is a turning point such

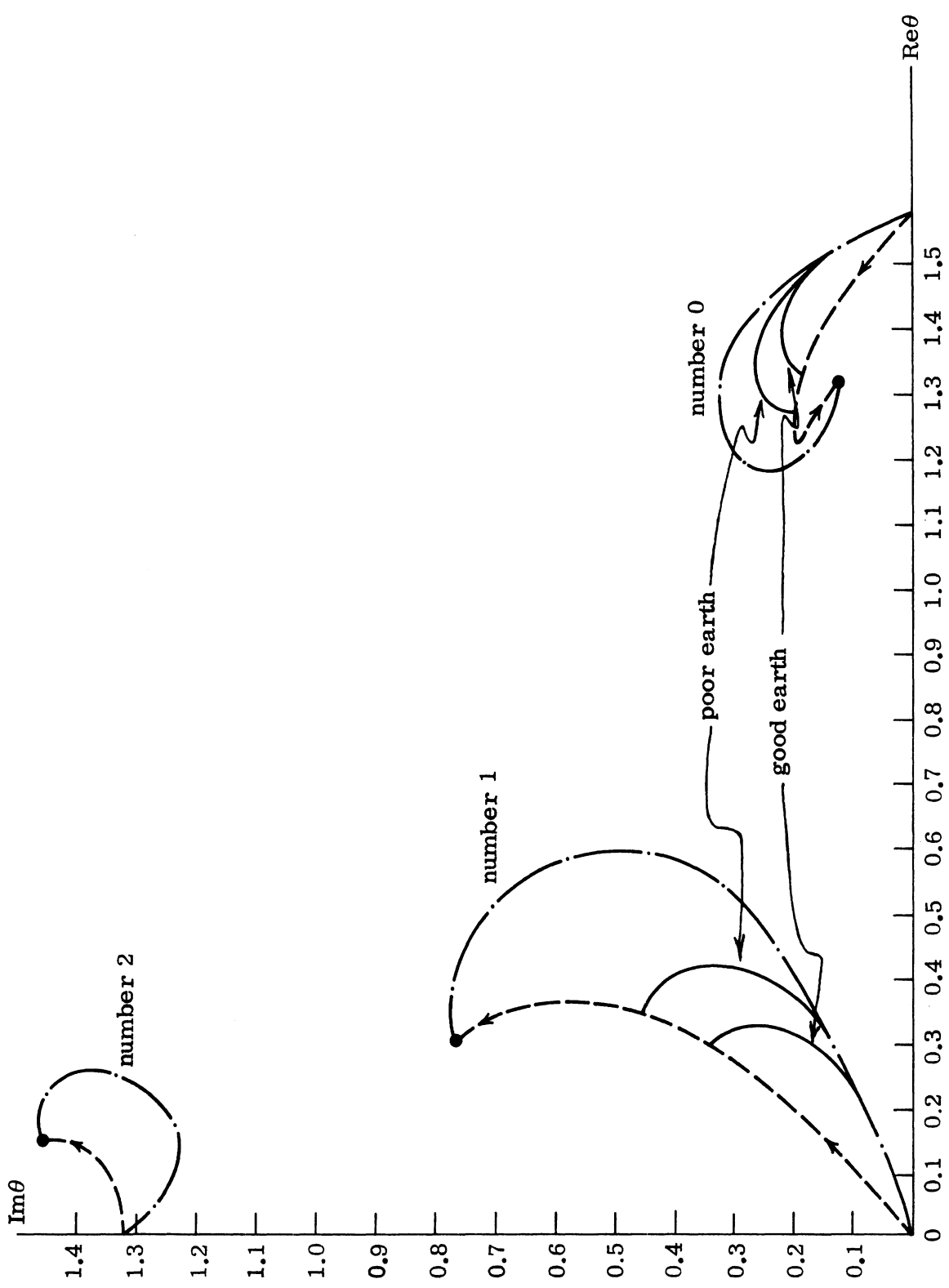


FIG. C-1: POLE LOCUS AT CUT-OFF FREQUENCY.

that the attenuation rate stops increasing as the refractive index becomes smaller. While the number 1 mode, on the contrary, rises rapidly as the refractive index decreases.

Figure C-2 presents the case for a frequency larger than cut-off. Except for the displacement of the number 1 pole, the shape of the pole locus remains almost the same. Each locus behaves in a similar fashion as before. It is obvious that for a frequency much larger than cut-off, there are more than two pole loci located near the real axis. The number 2 or higher numbered pole will behave like number 1, which has no turning point. For frequency less than cut-off, there exists only the number 0 pole near the real axis around $\theta = \pi/2$. Special attention should be given to this particular pole because sometimes it will never be swept through, as the case of good earth at 6 MHz, hence there is no surface wave related to it. In the literature, there is the common concept that the lower order mode dominates, which must be stated with care. In general, for a fixed frequency, the number 1 mode will dominate for large refractive index material. However, when the refractive index is smaller than a certain value, the number 0 mode will dominate. It is necessary to study the locus of the poles to assure a proper understanding and correct application of the mode theory.

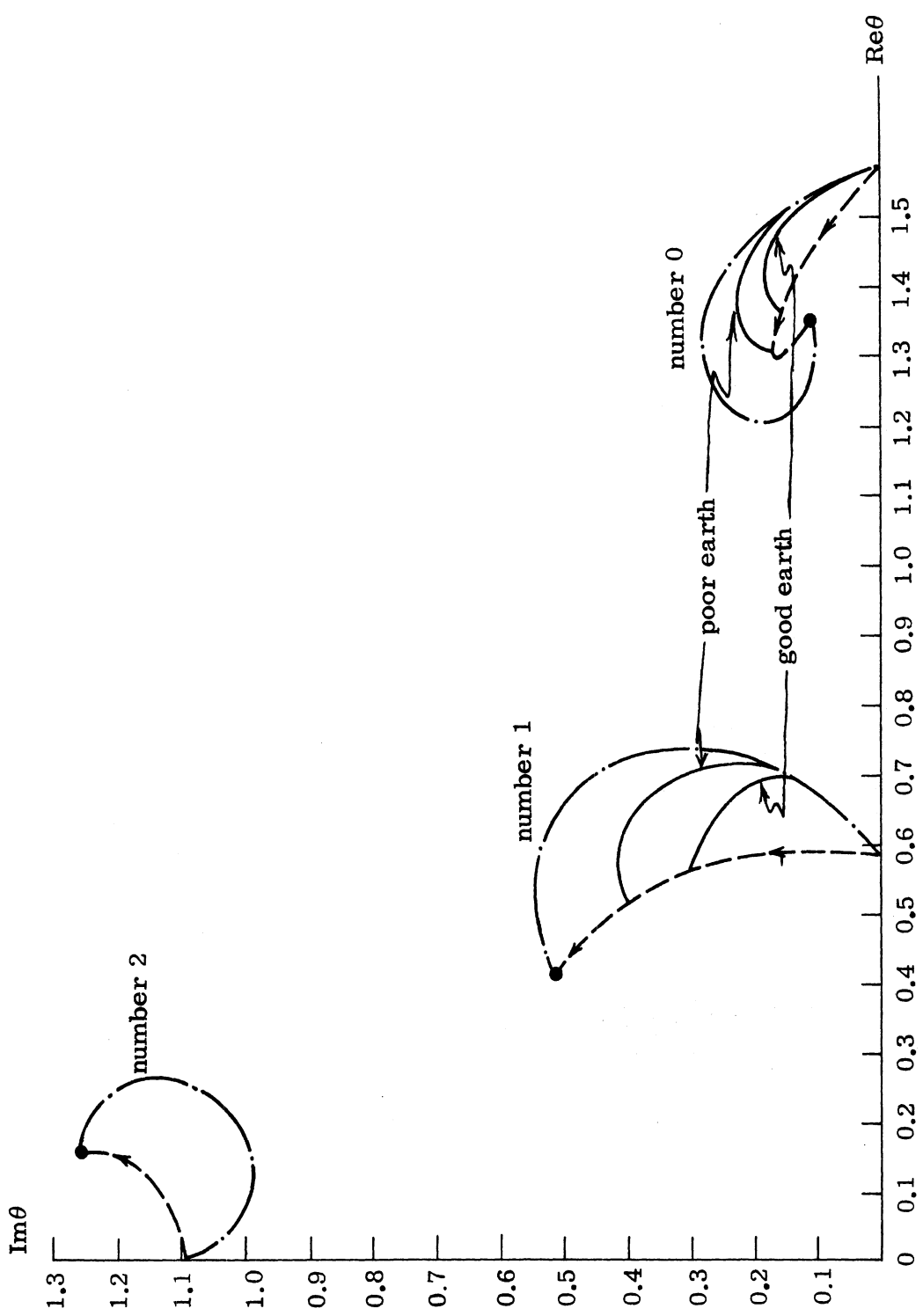


FIG. C-2: POLE LOCUS ABOVE CUT-OFF FREQUENCY.

APPENDIX D

COMPUTER PROGRAM

```
C *** PROGRAM FOR THE FAR-ZONE FIELD CALCULATION
C *** N**2=(A,B)=REFRACTIVE INDEX
C *** L=SEPARATION DISTANCE BETWEEN TWO INTERFACES
C *** K=WAVE NUMBER
C *** U=PERMEABILITY IN FREE SPACE
C *** Z0=POSITION OF THE SOURCE
C *** R=OBSERVATION POINT IN R-DIRECTION
C *** W=FREQUENCY USED
C *** EZ=FAR FIELD IN THE Z-DIRECTION
C *** ER=FAR FIELD IN THE R-DIRECTION
C *** EMZ=AMPLITUDE OF EZ
C *** EMR=AMPLITUDE OF ER
C *** EPHI=FAR FIELD IN THE PHI-DIRECTION(ONLY FOR PHI=
C *** 90 DEGREES)
C *** EMPHI=AMPLITUDE OF EPHI
C *** AEZ=APPROXIMATE FAR FIELD IN THE Z-DIRECTION
C *** AER=APPROXIMATE FAR FIELD IN THE R-DIRECTION
C *** AEPHI=APPROXIMATE FAR FIELD IN THE PHI-DIRECTION
C *** RM=REFLECTION COEFFICIENT
C *** RE=REFLECTION COEFFICIENT
C *** RMI=APPROXIMATE REFLECTION
C *** REI=APPROXIMATE REFLECTION
      REAL K,L,KL,KZ0
      COMPLEX P,SMUL,N,ER,EZ,EC,ASM,EPHI,AER,AEZ,RMUL,ARM
      *,RM,RMI,EXPR,RE,REI,EXPC,AEPHI,PEC
      PI=3.1415926
      A=4.
      B=0.3
      K=0.125663
      W=6.E6*2.*PI
      R=750.
      L=30.
      U=1.E-7/(4.*PI)
      KL=K*L
      COST=W*U/PI*10.**4
      R2=R**2
      N=CSORT(CMPLX(A,B))
      DO 10 LLL=1,5,4
      Z0=5.*LLL
      KZ0=K*Z0
      DO 10 M=1,31
      LL=M-1
      RR=SORT(R2+LL**2)
      RRKK=K*RR
      EXPR=CMPLX(COS(RRKK),SIN(RRKK))
      C=LL/RR
```

```

S=R/RR
CKL=KL*C
CC=COS(CKL)
SC=SIN(CKL)
EXPC=CMPLX(CC,SC)
CZ=COS(KZO*C)
P=CSQRT(CMPLX(A-S**2,B))
RM=EXPC*(CMPLX(A,B)*C-P)/(2.*P*CC-CMPLX(-B,A)*C*
*SC))
RMI=EXPC*(N*C-1.)/(2.*CC-CMPLX(0.,1.)*N*C*SC))
RMM=CABS(RM)
RMMI=CABS(RMI)
WRITE(6,20)
20 FORMAT('-
        WRITE(6,51)RM,RMI
        WRITE(6,102)RMM,RMMI
        SMUL=(CMPLX(A,B)*C*CC-CMPLX(0.,1.)*P*SC)/(P*CC-CMP
*LX(-B,A)*C*SC)
        SMMUL=CABS(SMUL)
        WRITE(6,107)SMUL,SMMUL
        ASM=(CMPLX(0.,1.)*SC-C*CC*N)/(CMPLX(0.,1.)*N*C*S
*C-CC)
        AMSM=CABS(ASM)
        WRITE(6,108)ASM,AMSM
        IF(I,L,E0,0)GO TO 13
        RE=(C-P)*EXPC/(2.*C*CC-CMPLX(0.,1.)*P*SC))
        REI=(C-N)*EXPC/(2.*C*CC-CMPLX(0.,1.)*N*SC))
        RME=CABS(RE)
        RMEI=CABS(REI)
        WRITE(6,52)RE,REI
        WRITE(6,102)RME,RMEI
        RMUL=(CMPLX(0.,-1.)*C*SC+P*CC)/(C*CC-CMPLX(0.,1.)*
**P*SC)
        RMMUL=CABS(RMUL)
        WRITE(6,105)RMUL,RMMUL
        FORMAT('SUM OF RE',3E12.5)
        ARM=(N*CC-CMPLX(0.,1.)*C*SC)/(CMPLX(0.,-1.)*N*SC+
*C*CC)
        AMRM=CABS(ARM)
        WRITE(6,106)ARM,AMRM
        PEC=CONST*EXPR*SIN(KZO*C)/RR
        EPHI=PEC*(1+RMUL)
        EMPHI=CABS(EPHI)
        AEPHI=PEC*(1+ARM)
        AEMPHI=CABS(AEPHI)
        WRITE(6,101)EPHI,AEPHI
        WRITE(6,102)EMPHI,AEMPHI

```

```
13  CONTINUE
106  FORMAT('ARM ',3E12.5)
107  FORMAT('SUM OF RM',3E12.5)
108  FORMAT('ASM ',3E12.5)
      EC=COST*S*CZ*CMLX(0.,1.)*EXPR/RR
      EZ=-EC*S*(1+SMUL)
      ER=EC*C*(1+SMUL)
      EMZ=CARS(EZ)
      EMR=CARS(ER)
      AEZ=-EC*S*(1+ASM)
      AER=EC*C*(1+ASM)
      AEMZ=CARS(AEZ)
      AEMR=CARS(AER)
100  FORMAT(1X,I2,2X,8E12.5)
      WRITE(6,102)EMR,EMZ,AEMR,AEMZ
102  FORMAT(8X,E12.5,10X,E12.5,10X,E12.5,12X,E12.5)
51  FORMAT('MUL REF COEFF  RM',4E12.5)
52  FORMAT('MUL REF COEFF  RE',4E12.5)
101  FORMAT('MEPHI ',4E12.5)
10  WRITE(6,100)LL,ER,EZ,AER,AEZ
      STOP
      END
```

```

C *** THIS PROGRAM IS SUGGESTED TO BE USED ON THE TERMINA
C     L FOR THE SEARCHING OF POLES IN THE COMPLEX THETA
C     PLANE FOR 'TM' WAVES SINCE IMPROPER CHOICE OF SU
C     LUTIONS MAY NOT CONVERGE
C *** K=WAVE NUMBER
C *** L=SEPARATION DISTANCE BETWEEN TWO INTERFACES
C *** N**2=(A,B)=REFRACTIVE INDEX
C *** LE=EIGENVALUE IN THE X-DIRECTION
C *** HL=EIGENVALUE IN THE Z-DIRECTION
REAL K,L
COMPLEX LE,HL
A=1.02
B=0.3
K=0.125663
L=30.
C *** ARBITRARILY CHOOSE A PAIR OF SOLUTIONS
20 READ(5,1000)X,Y
AL=K*L
1 SX=SIN(X)
SHY=SINH(Y)
CX=COS(X)
CHY=COSH(Y)
CS=CX*SHY
SC=SX*CHY
CC=CX*CHY
SS=SX*SHY
C=A-SC**2+CS**2
D=B-2*CC*SS
P=SQR T(C**2+D**2)
Q=1./P
PM=SORT(P-C)
PP=SORT(P+C)
PMQ=1./PM
PPO=1./PP
PCR=-2.*SX*CX*(SHY**2+CHY**2)
PCI=2.*SHY*CHY*(CX**2-SX**2)
ACC=AL*CC
ASS=AL*SS
ACS=AL*CS
ASC=AL*SC
F=1.414214*((A*CC+B*SS)*TANH(ASS)-(B*CC-A*SS)*TAN
*(ACC))-PP+PM*TAN(ACC)*TANH(ASS)
G=1.414214*((A*CC+B*SS)*TAN(ACC)+(B*CC-A*SS)*TANH
*(ASS))-PM-PP*TAN(ACC)*TANH(ASS)
C *** PREASSIGN VALUES AS THE TOLLENCE FOR THE CONVERGENCE
IF(ABS(F).LT. 0.001 .AND. ABS(G).LT. 0.001) GO
*TO 11
FPR=1.414214*(TANH(ASS)*(-A*SC+B*CS)+(A*CC
*+B*SS)*(ACS)/(COSH(ASS))

```

```

*) )**2)+(ASC)*(B*CC-A*SS)/((COS(ACC))**2)+  

*TAN(ACC)*(B*SC+A*CS))-0.5  

**PPQ*(PCR+Q*(C*PCR-D*PCI))+0.5*PMQ*(-PCR+Q*  

*(C*PCR-D*PCI))*TAN(ACC)  

**TANH(ASS)+PM*((TANH(ASS)*(-ASC))/((COS(ACC))**  

**2)+(ACS)*TAN(ACC)/((COSH(ASS))**2))  

FPI=1.414214*(TAN(ASS)*(A*CS+B*SC)+(A*CC+B  

**SS)*(ASC)/((COSH(ASS))**2))  

***2)-(ACS)*(B*CC-A*SS)/((COS(ACC))**2)-TAN(AC  

*C)*(B*CS-A*SC))-0.5*  

*PPQ*(PCI+Q*(C*PCI+D*PCR))+0.5*PMQ*  

*(-PCI+Q*(C*PCI+D*PCR))  

**TAN(ACC)*TANH(ASS)+PM*((ACS)*TANH(ASS)/((COS(AC  

*CC))**2)+(ASC)*TAN(ACC)/((COSH(ASS))**2))  

GPR=1.414214*((-ASC)*(A*CC+B*SS)/((COS(ACC  

*) )**2+TAN(ACC)*(-A*SC  

*+B*CS)+(ACS)*(B*CC-A*SS)/((COSH(ASS))**2)+TA  

*NH(ASS)*(-B*SC-A*CS  

*) -0.5*PMQ*(-PCR+Q*(C*PCR-D*PCI))-0.5*PPQ*  

*(PCR+Q*(C*PCR-D*PCI))  

**TAN(ACC)*TANH(ASS)-PP*((-ASC)*TANH(ASS)/((COS(A  

*CC))**2)+TAN(ACC)*ACS/((COSH(ASS))**2))  

GPI=1.414214*((ACS)*(A*CC+B*SS)/((COS(ACC  

*) )**2)+TAN(ACC)*(A*CS  

*+B*SC)+(ASC)*(B*CC-A*SS)/((COSH(ASS))**2)+  

*TANH(ASS)*(B*CS-A*SC))  

*+0.5*PMQ*(PCI-Q*(C*PCI+D*PCR))-0.5*PPQ*(PC  

*I+Q*(C*PCI+D*PCR))*TAN  

*(ACC)*TANH(ASS)-PP*((ACS)*TANH(ASS)/((COS(ACC  

*) )**2)+(ASC)*TAN(ACC)/((COSH(ASS))**2))  

DD=FPR*GPI-FPI*GPR  

DX=(G*FPI-F*GPI)/DD  

DY=(F*GPR-G*FPR)/DD  

WRITE(6,10)X,Y,F,G  

X=X+DX  

Y=Y+DY  

GO TO 1
11 WRITE(6,10)X,Y,F,G
LED=K*(SC+(0.,1.)*CS)
HL=ACC+(0.,-1.)*ASS
WRITE(6,12)LED
WRITE(6,12)HL
GO TO 20
10 FORMAT(2X,E11.4,2X,E11.4,2X,E10.3,2X,E10.3)
1000 FORMAT(2F11.5)
12 FORMAT(2X,2E12.5)
STOP
END

```